Dear Proceedings of the National Academy of Sciences editorial board,

We are submitting our manuscript entitled “Mechanical performance of hybrid polymer-lipid vesicles with leaflet asymmetry engineered using microfluidics” by Yuting Huang, Arash Manafirad, Simon Matoori, Laura R. Arriaga, Sije Sun, Anqi Chen, Anthony D. Dinsmore, David J. Mooney, and David A. Weitz for publication in PNAS.

Lipid vesicles, an aqueous core enclosed by a lipid bilayer, are ubiquitous in human bodies. They are also engineered as state-of-the-art drug delivery vehicles. The incorporation of polymers into these bilayers, named hybrid polymer-lipid vesicles, significantly bolsters the stability and surface functionality of these vesicles. Intriguingly, the polymers and lipids can adopt an asymmetric distribution between two leaflets in the bilayer, consequently further modifying the vesicle properties, leading to properties unattainable in symmetric vesicles. However, the effect of leaflet asymmetry on the vesicle property remains largely elusive because of the arduous task of creating hybrid vesicles with precisely controlled compositions and leaflet asymmetry. In this paper, we use microfluidics to fabricate hybrid vesicles with fine-tuned composition and leaflet asymmetry, enabling us to analyze the effect of these parameters systematically using micropipette aspiration and fluorescent imaging-based techniques. Remarkably, we find that the asymmetric vesicles are an order of magnitude stiffer and several times tougher than their symmetric counterparts. Furthermore, asymmetric vesicles exhibit a significant reduction in membrane fluidity and permeability. We attribute these property changes to the unique structure of the asymmetric vesicles: a rigid polymer leaflet supported by a stretchable lipid leaflet. Together, these two leaflets synergistically improve the overall bilayer stability. Additionally, the continuous polymer leaflet protects the encapsulated substance from escaping through leaky lipid patches. Overall, our study highlights the exceptional role that leaflet asymmetry plays in modulating the properties of vesicles.

Hybrid polymer-lipid vesicles are promising for usage in pharmaceuticals, biosensors, and biophysical studies; introducing leaflet asymmetry greatly broadens its utility. Thus, we believe this paper could appeal to a wide audience interested in both fundamental vesicle properties and their applications, suitable to be published in the Journal of PNAS.

Mechanical performance of hybrid polymer-lipid vesicles with leaflet asymmetry engineered using microfluidics

Yuting Huang[1], Arash Manafirad[2], Simon Matoori[1,3], Laura R. Arriaga[4], Sijie Sun[1], Anqi Chen[1], Anthony D. Dinsmore[2], David J. Mooney[1,5], and David A. Weitz[1,5*]

1. John A. Paulson School of Engineering and Applied Sciences Harvard University, Cambridge, MA, 02138, USA
2. Department of Physics, University of Massachusetts Amherst, Amherst, MA, 01003, USA
3. Faculté de Pharmacie, Université de Montréal, Montreal, Quebec H3T 1J4, Canada
4. Department of Theoretical Condensed Matter Physics, Condensed Matter Physics Center and Instituto Nicolás Cabrera, Universidad Autónoma de Madrid, 28049, Madrid, Spain
5. Wyss Institute for Biologically Inspired Engineering, Harvard University, Boston, MA, 02115, USA.

Corresponding author email*: weitz@seas.harvard.edu

Competing Interest Statement: There is no competing interest.

Classification: Physical Sciences (major); Applied Physical Sciences (minor)

Keywords: Microfluidics, hybrid polymer-lipid vesicles, asymmetrical leaflets, mechanical properties

Abstract:

Lipid vesicles consist of aqueous cores surrounded by a bilayer of phospholipids. Hybrid polymer-lipid vesicles incorporate both polymers and lipids, offering promising properties for developing pharmaceuticals, biosensors, and artificial cells. The hybrid vesicles can be symmetric, in which their two leaflets contain identical compositions, or asymmetric, in which the leaflets possess dissimilar compositions and can lead to dramatically modified properties. However, methods to produce both symmetric and asymmetric hybrid vesicles result in heterogenous compositions and sizes, making it challenging to quantify the effect of asymmetry and limiting applications. Here, we use a microfluidic approach to produce hybrid vesicles containing symmetric or asymmetric leaflets with precisely engineered compositions. We find the vesicles with asymmetric leaflets are significantly stiffer and tougher than those with symmetric leaflets; moreover, the lateral diffusivity of lipids is greatly decreased. The optimum structure consists of an inner leaflet that is a stretchable lipid leaflet and an outer leaflet that is a fully continuous polymer leaflet. This technique of precisely engineering asymmetric structures can be applied to hybrid vesicles composed of other types of polymers and lipids, further expanding their potential applications.

Significance Statement

Vesicles, which consist of aqueous cores surrounded by lipid bilayers, are widely explored for drug encapsulation and delivery due to their resemblance to cell membranes. Polymersomes, formed from bilayers of block copolymers, offer enhanced performance through their synthetic and expanded material properties but lack the biocompatibility of lipid vesicles. Hybrid polymer-lipid vesicles combine the biocompatibility of lipids with the chemical versatility of polymers. Here, we report a novel method for producing asymmetric vesicles with distinct lipid and polymer leaflets that offer even greater advantages. These vesicles are nearly as stiff as polymersomes yet much tougher, and they are as resistant to leakage as polymersomes while maintaining biocompatibility for drug delivery, thanks to their lipid based inner leaflet.

Introduction

Lipid vesicles consist of aqueous cores surrounded by a bilayer of phospholipids; they are intrinsically biocompatible and widely used as delivery vehicles for pharmaceuticals, food, and cosmetics (1-8). However, lipid vesicles suffer from poor mechanical stability and limited chemical functionality (9-12). By comparison, polymersomes are synthetic analogs of lipid vesicles made from much larger amphiphilic polymers(13, 14). Polymersomes can exhibit properties differing by one or multiple orders of magnitude, greatly extending the application of lipid vesicles (15-17). Despite the improved mechanical robustness, polymersomes possess limited biocompatibility, which hinders their usage in biotechnology (9-12, 18). Hybrid polymer-lipid vesicles consist of a bilayer of polymer and lipid mixtures; they have the potential advantage of combining the biocompatibility of lipid vesicles with the chemical versatility of polymersomes (9-12, 19-27). Their properties, however, are not understood due to the difficulty in assembling and assessing them. With drastically different chemistry and size, the polymers and lipids can arrange into different microstructures, which lead to an array of properties unattainable in lipid vesicles and pure polymersomes(10-12, 22, 28-35). Depending on the type of polymer and the volume ratio between polymers and lipids, the hybrid vesicles can possess properties either in between or exceeding the range exhibited by lipid vesicles and polymersomes(19, 20, 29, 36-42). The vesicles can possess symmetric membranes, where the polymers and lipids are identical in each monolayer. The polymers and lipids can homogeneously mix when the entropy dominates over the chemical potential, or phase separate when the potential energy gain of assembly outweighs the entropy gain(27, 28, 38, 39, 43, 44). The vesicles can possess asymmetric membranes, where the two monolayers contains dissimilar compositions(6, 45-50). The individual structure of each monolayer, together with their coupling, determines the property of the vesicle. The asymmetric structure introduces a new degree of complexity to vesicles (51-64). Conventional methods, such as rehydration and electroformation, struggle to control the size, composition, and structure of vesicles(10, 44, 49). How these intricate microstructures dictate the macroscopic properties remains elusive. Thus, the absence of both a controlled assembly method and a thorough study of vesicle properties hinders the potential for many applications.

In this work, we produce the hybrid vesicles with controlled membranes, both symmetric and asymmetric, and analyze their mechanical properties. We generate the vesicles using a novel multiple emulsions approach, made with microfluidics, which enables engineering each leaflet to have precise compositions. Symmetric vesicles are

made from water-in-oil-in-water double emulsions, while asymmetric vesicles are made from triple emulsions, with a water core surrounded by two oil shells. Using micropipette aspiration, we find that asymmetric hybrid vesicles possess an enhanced stretching modulus and toughness as compared to symmetric hybrid vesicles. Using Fluorescence Recovery After Photobleaching (FRAP), we determine that the lipid diffusion coefficient is lower in asymmetric hybrid vesicles as compared to that in symmetric hybrid vesicles, even when the amounts of polymer are similar in the vesicles. Membrane permeability test further shows reduced permeability in asymmetric vesicles as compared to symmetric vesicles. To account for the results, we propose that symmetric hybrid vesicles possess lipid domains dispersed in between polymer domains, leading to their lower membrane stiffness and toughness. By contrast, asymmetric hybrid vesicles possess one stiff polymer leaflet and one stretchable lipid leaflet, which give rise to their significantly higher stiffness and toughness.

Results and Discussion

Microfluidic Production of W/O/W Double Emulsion Templated Symmetric Hybrid Vesicles and Their Fluorescence Characterization

To fabricate symmetric polymer-lipid vesicles, we use a glass capillary microfluidics device to generate water-in-oil-in-water (W/O/W) double emulsions as templates for vesicles(65, 66). The device comprises of two cylindrical capillaries, each with a tapered end, axially aligned inside a square capillary. The left cylindrical capillary contains an even smaller capillary, as illustrated by the schematic in Figure 1A (top). We render the left cylindrical capillary hydrophobic by treating it with n-octadecyl-trimethoxy silane and the right cylindrical capillary hydrophilic by treating it with 2-[methoxy (polyethyleneoxy) propyl] trimethoxy silane. During operation, we introduce an aqueous phase containing 10 wt% poly(ethylene glycol) (PEG) through the innermost capillary from the left-hand side at a flow rate of 300 µl/hr. This PEG solution significantly enhances the optical contrast between the double emulsion cores and the outer aqueous media. Simultaneously, we inject an oil phase containing 80 wt% 1,2-dioleyl-sn-glycero-3-phosphocholine (DOPC) and 20 wt% 10 kDa poly(ethylene glycol)-block-15 kDa poly(D,L-lactic acid) (PEG-b-PLA) , dissolved at 5 mg/ml in a mixture of 36 vol% chloroform and 64 vol% hexane, through the left tapered capillary at the same flow rate. The hydrophobic coating on the left capillary allows large water-in-oil emulsions to form inside the capillary, as shown in Figure 1A. Next, we inject 10 wt% poly(vinyl alcohol) (PVA) through the right tapered capillary at a flow rate of 3000 µl/hr. The hydrophilic coating on the right capillary prevents the middle oil phase from wetting its surface.

Under these conditions, W/O/W double emulsions with an outer diameter of 80 µm form at the junction between the right and left capillaries, as depicted in the bright-field image in Figure 1A (bottom). We collect these vesicles in a solution composed of 50 vol% PBS buffer and 50 vol% water, ensuring the same osmolarity as the inner phase. To assess the uniformity of the vesicles, we capture optical images and analyze their diameters using a contour detection algorithm developed in MATLAB. Our analysis reveals that the collected double emulsions exhibit a coefficient of variation (CV) of approximately 5.2%, as illustrated in Figure 1B. This level of uniformity is consistent with the range reported for vesicles produced by other microfluidic techniques. We use these double emulsions as templates for symmetric hybrid vesicles. The PEG-b-PLA and DOPC, immersed in the middle oil shell, adsorb to the interfaces between the aqueous phase and the oil phase; as the oil leaves the membrane, the two interfaces come into contact to form polymer-lipid vesicles with symmetric leaflets, as illustrated by Figure 1C. When viewed under the microscope, the oil shells in double emulsions appear to become thinner and exit the membrane in the form of oil bubbles (66, 67), allowing the double emulsions to form vesicles, as shown by the bright field images in Figure 1D. Importantly, DOPC is a fluid-phase lipid at room temperature, whereas PEG-b-PLA is a solid-phase polymer(67-75). This combination of fluid-like and solid-like components introduces a new level of complexity in the membranes, akin to the complexity found in cell membranes(76-82). Furthermore, PEG-b-PLA is more than ten times larger than DOPC, resembling the way small molecules are embedded with large proteins in cell membranes. This size disparity allows us to explore how significant differences in molecular sizes influence the overall properties of the membrane. To characterize the distribution of polymers and lipids within the membrane, we incorporate 3 wt% of the lipophilic dye 1,2-dioleoyl-sn-glycero-3-phosphoethanolamine-N-(lissamine rhodamine B sulfonyl) (18:1 Liss Rhod PE) into the lipid leaflet, and 3 wt% of the block copolymer dye fluorescein isothiocyanate-PEG-b-PLA (FITC-PEG 5000 Da-b-PLA 10000 Da) into the polymer leaflet. We then examine the vesicles using confocal microscopy with a 10X objective. This method reveals a uniform distribution of both dyes across the vesicle surface, as shown in Figure 1E. The lipids are thus embedded in between polymers throughout the membrane. The fluid phase lipid DOPC likely facilitates the distribution of the solid phase PEG-b-PLA across the

vesicle surface. Using confocal microscope with a10X objective, we cannot detect any phase separation of polymers and lipids; however, separate polymer and lipid domains exist below the resolution of the objective. To investigate how the solid phase of lipids affects the overall membrane, we incorporate 40 wt% DPPC, a solid-phase lipid at room temperature, into the membrane fabrication. The resulting membrane is comprised of 40 wt% DPPC, 40 wt% DOPC, and 20 wt% PEG-b-PLA, as shown in Figure 1F. Additionally, we include 3 wt% naphthopyrene, which associates with DPPC-rich domains, and 3 wt% 18:1 Liss Rhod PE, which associates with DOPC-rich domains. Using confocal microscopy, we observe a phase-separated membrane, where red fluorescence indicates DOPC-rich domains, blue fluorescence highlights DPPC-rich domains, and non-fluorescent regions represent polymer-rich domains, as depicted in Figure 1F. These observations lead us to conclude that solid lipids and solid polymers phase-separate more readily than liquid lipids and solid polymers. Liquid lipids likely promote uniform distribution of molecules through faster diffusion. This study demonstrates a versatile microfluidic approach for creating symmetric polymer-lipid vesicles, applicable to various formulations.

Microfluidic Production of W/O1/O2/W Triple Emulsion Templated Asymmetric Hybrid Vesicles and Their Fluorescence Characterization

To make asymmetric hybrid vesicles, we employ a novel approach using the same device that produces symmetric hybrid vesicles but modify the procedure to produce water-in-oil-in-oil-in-water (W/O/O/W) triple emulsions. During the operation, we introduce an aqueous phase, containing 10 wt% PEG, through the innermost capillary from the left-hand side at a flow rate of 300 $\mu l/hr$. Simultaneously, we inject an oil phase containing DOPC at a concentration of 8 mg/ml through the left cylindrical capillary at the same flow rate. Additionally, a second oil phase containing PEG-b-PLA at the same concentration is injected through the gap between the left cylindrical capillary and the outermost square capillary, also at a flow rate of 300 $\mu l/hr$. We then flow an outermost aqueous phase containing 10 wt% PVA at a flow rate of 3000 $\mu l/hr$ from the opposite side, as shown by Figure 2A. The oil phases are composed of the same chloroform and hexane solvents as used to produce symmetric hybrid vesicles. Under these conditions, W/O/O/W triple emulsions with an outer diameter of 80 μm form between the tapered capillaries, as shown by the bright field image in Figure 2A**.** We collect these vesicles in a solution containing 50 vol% PBS buffer and 50 vol% water, ensuring that the outer media matches the osmolarity of the inner aqueous cores. To assess the uniformity of the vesicles, we capture optical images and analyze their diameters using a contour detection algorithm developed in MATLAB. Our analysis reveals that the collected triple emulsions exhibit a coefficient of variation (CV) of approximately 5.5%, as shown in Figure 2B. This level of uniformity is consistent with the range reported for vesicles produced by other microfluidic techniques. We use these triple emulsions as templates for asymmetric hybrid vesicles. The PEG-b-PLA in the outer oil shell predominantly diffuses to the outer water-oil interface, while DOPC in the inner shell migrates mainly to the inner water-oil interface. As the oil exits the membrane, the two interfaces come into contact, resulting in the formation of a polymer-lipid vesicle with asymmetric leaflets. This process forces the oil to dewet from the membrane, as illustrated in Figure 2C. Under the 10x objective, we observe the oil exiting the triple emulsions by forming oil caps at a contact angle to the membrane, as depicted by the bright-field images in Figure 2D. The contact angle and large oil cap reflect the strong attractive forces between the interfaces, facilitating bilayer formation. Moreover, to investigate the molecular distribution within the membrane, we incorporate 3 wt% of a red fluorescent lipid, 18:1 Liss Rhod PE, and 3 wt% of a green fluorescent polymer, FITC-PEG-b-PLA, into the membrane. Using confocal microscopy, we observe a uniform distribution of both the lipid and polymer across the membrane, as indicated by the consistent red and green fluorescence shown in Figure 2E. This result suggests that the lipids and polymers are distributed throughout the membrane, likely in separate leaflets.

To characterize bilayer asymmetry, we measure the degree of asymmetry, defined as the percentage of molecules that remain asymmetrically distributed in the bilayer (6, 83-85). For vesicles with polymer inner and lipid outer leaflets, labeled as formulation F4, we incorporate 3 wt% of fluorescent lipids, 1,2-dioleoyl-sn-glycero-3-phosphoethanolamine-N-(7-nitro-2-1,3-benzoxadiazol-4-yl) (ammonium salt) (DOPE-NBD), into the lipid outer leaflet during fabrication. We then add a 1M dithionite solution, a quencher for DOPE-NBD, and observe the fluorescence under confocal microscopy five minutes post-addition. The fluorescence signal of the vesicles drops to 34%, as shown by the right images in Figure 2F. Further addition of a salt solution causes the vesicles to break, completely extinguishing the fluorescence. These results suggest that 34% of DOPE-NBD resides in the inner leaflet, while 66% remains in the outer leaflet, resulting in a degree of asymmetry of 66% for these vesicles. To investigate the degree of asymmetry in vesicles with lipid inner and polymer outer leaflets, labeled as formulation F5, we switch the two oils during production and incorporate 3 wt% of DOPE-NBD into the inner DOPC leaflet. After

adding a 1M dithionite solution, we observe that the fluorescence signal of these vesicles drops to 78%, as shown by the left images in Figure 2G. Subsequent addition of a salt solution with higher osmotic pressure than the vesicle cores cause the vesicles to break, fully extinguishing the fluorescence. These findings indicate that 78% of DOPE-NBD is in the inner leaflet, while 22% is in the outer leaflet, resulting in a degree of asymmetry of 78% for these vesicles. The higher degree of asymmetry in formulation F5 compared to F4 could be attributed to the increased polymer introduction from the thick outer oil shell, leading to fewer lipids being incorporated into the membrane and thus higher asymmetry.

Mechanical Properties of the Vesicles Assessed by Micropipette Aspiration Measurments

To study the mechanical properties of the vesicles, we conduct micropipette aspiration measurements (39, 86-96). Our vesicles are slightly inflated, with an inner osmolarity that is 20 mOsmo higher than that of the outer aqueous media. For the measurements, a vesicle is aspirated into the mouth of the pipette, which has a radius of R_p, by applying a suction pressure ΔP , as shown by the schematic and images in the first row in Figure 3A. This suction pressure provides a tensile stress on the vesicle membrane, causing its surface area to expand. Then, the vesicle has a projected length of L inside the micropipette and a radius of R_s outside of the micropipette, as shown by the schematic and images in the second row in Figure 3A. Due to the short duration of the experiment, the volume of the vesicle remains constant, allowing us to determine the areal strain, α, optically from R_p, R_s , L, and the initial vesicle area A_o, using the equation, $\alpha = \frac{2\pi R_p L}{A_o}(1 - \frac{R_p}{R_s})$ (96). Since the pressure is uniform in the interior of the vesicle, the membrane curvatures enable us to determine the membrane tension τ using the Laplace equation, $\tau = \frac{\Delta P}{2\left(\frac{1}{R_p} - \frac{1}{R_s}\right)}$ (96). We incrementally increase ΔP and determine the strain dependence of the tension. The slope of the tension versus strain curve represents the stretching modulus, while the area under the curve represents the toughness. Using this procedure, we formulate a range of vesicles. These include symmetric vesicles, labeled F1 to F3, with polymer content increasing from 0 wt% to 80 wt%, and asymmetric vesicles, labeled F4 to F5, with degrees of leaflet asymmetry increasing from 66% to 78% in opposite leaflet configurations. Additionally, we prepare a pure polymersome, labeled F6. The details are summarized in the table in Figure 3B.

To investigate the effect of composition on the mechanical properties of the vesicles, we examine their tension versus strain curves. As a reference, we consider the DOPC vesicles, labeled F1. We find that the tension versus strain relationship is linear, as evidenced by the light blue colored curve in Figure 3C. This behavior is typical for fluid vesicles in the areal expansion regime. As we increase the polymer fraction in vesicles to 20 wt%, the data exhibit a sharper initial linear rise, indicating a much larger stretching modulus at low strain, as shown by comparing the light blue and purple curves in the inset. However, at higher strains, the slope of the increase becomes comparable to, or even less than, that of the pure DOPC, by comparing the light blue and purple curves, labeled F2, in Figure 3C. This behavior suggests that the small amount of polymer initially forms a network with a larger modulus than DOPC. However, at larger strains, this network breaks into separated islands that remain disconnected. As a result, the stretching modulus at larger strains is determined primarily by DOPC, with the contribution of the polymer islands being negligible.

When we increase the polymer fraction to 80 wt%, there is a threshold tension at which strain is observed, indicating that the vesicle is initially solid (describe, a separate sentence, there is shear force necessary to deform the vesicle indicating it's solid). as shown by the green curve, labeled by F3, in the insert of Figure 3C. As the strain increases above zero, there is a linear behavior with a slope that is greater than that of the vesicles with lower amounts of polymer; at even larger strains, the slope decreases and becomes roughly comparable to that of both the vesicles with lower amounts of polymers and the DOPC vesicles, as shown in the figure 3C. This behavior suggests that the vesicle with 80 wt% polymer, after the initial yielding, remains a stiff solid consisting of large polymer networks; at even greater strains, the polymer networks break and the behavior is dominated by the remaining lipid phase.

To explore how leaflet asymmetry impacts the mechanical properties, we measure vesicles with polymer on the inside and lipid on the outside, labelled as F4, which possess 66% asymmetry of the lipids. The data exhibit an initial linear rise followed by a linear regime that increases more slowly at much larger strains, as depicted by the yellow curve in Figure 3C. The slope of the initial rise is greater than that of the DOPC vesicles, indicating that the polymers in one leaflet are forming a network leading to increased stiffness. The DOPC lipids in the other leaflet

maintain the fluidity of the whole vesicle and allow it to deform without shear resistance. As the membrane expands, the polymers network breaks into polymer islands separated by lipids both in its own leaflet and the opposite leaflet, as manifested by the more slowly increasing linear regime at larger strains. Finally, we measure the asymmetric vesicles with polymer outside and lipid inside, which possess 78% asymmetry. The data exhibit a sharp rise at zero strain and a significantly steeper slope, as shown by the red curve in Figure 3C. The sharp rise at zero strain indicates that the polymers in the one leaflet form a fully continuous solid and the steeper slope shows a greatly increased stretching modulus as compared to the vesicles with a lower degree of asymmetry. As the membrane expands, the polymer network expands but does not break into polymer islands, as shown by the smooth transition of slope at higher strains. To validate our hypothesis, we measure polymersomes consisting of two fully continuous polymer leaflets. Notably, we find the slope of the data, which measures the stretching modulus, to have a value approximately two to three times as large as the vesicle with a higher degree of asymmetry, as shown by the dark blue curves in Figure 3C. The approximate doubling in slope is consistent with our hypothesis that the vesicle with a higher degree of asymmetry possesses one fully continuous polymer leaflet.

To confirm the fluid or solid state of the vesicles, we examine optical images of vesicles at the moment of rupture, as shown in Figure 3D. Vesicles composed of DOPC lipids, symmetric hybrid vesicles composed of 20 wt% polymers, and asymmetric vesicles with 66% asymmetry all display smooth membranes upon breaking, consistent with both leaflets being fluid-like, as depicted by F1, F2, and F4 in Figure 3D. In contrast, symmetric hybrid vesicles with 80 wt% polymer, asymmetric hybrid vesicles with 78% asymmetry, and polymersomes all exhibit wrinkles upon breaking. This observation indicates that at least one leaflet is solid-like, as shown by F3, F5, and F6 in Figure 3D.

To show the statistics of vesicle properties, we plot the mean and standard deviation of stretching modulus and lysis strains for all groups of vesicles. Interestingly, the highly asymmetric vesicles, lablled as F6, exhibit an order of magnitude higher stretching modulus than all symmetric hybrid vesicles, labelled as F1 to F3, while possessing several times higher of lysis strain than polymersomes, labelled as F5, as shown by Figure 3E. These results indicate the significant impact of leaflet asymmetry on modulating vesicle properties.

To show the statistics of vesicle stability, we plot their lysis tension and toughness obtained from the areas below the tension versus strain curves. As the polymer fraction increases, both the lysis tension and toughness increase, as depicted by F1, F2, and F3 in Figure 3F. Interestingly, as the degree of asymmetry increases, both the lysis tension and toughness increase much more drastically, where the toughness is much larger than that of the polymersomes, as shown by comparing F4, F5, and F6 in Figure 3F. We conclude that the asymmetric leaflet structure optimizes toughness and maintains high stiffness, likely due to its fully continuous polymer leaflet providing the stiffness and its lipid leaflet contributing to the stretchability.

Lipid Diffusion in Vesicle Membrane Assessed by Fluorescence Recovery after Photobleaching (FRAP) Measurements

To investigate the presence of domains exist in symmetric versus asymmetric vesicles, we employ Fluorescence Recovery After Photobleaching (FRAP) to determine lipid mobilities (97-104). We label the membranes with 2 mol% of the lipophilic fluorescent dye 1,2-dioleoyl-sn-glycero-3-phosphoethanolamine-N-(carboxyfluorescein) (ammonium salt) (DOPE-carboxy fluorescein). By focusing an intense laser on a circular area of the membrane, we photo-bleach the fluorescent lipids within this region. We then observe the gradual recovery of fluorescence in the bleached area due to the diffusion of unbleached molecules, as illustrated by both the schematics and images for a DOPC vesicle in Figure 4A. We measure the recovered fluorescence intensity in the bleached area, $I_b(t)$, over time *t* by averaging the pixel intensities within the region, as illustrated by the red circle in the images in Figure 4A. We also track the fluorescence intensity in a control area in the unbleached region, $I_c(t)$, with the same radius as the bleached circular disk, as indicated by the blue circle in the images in Figure 4A. We determine the normalized fluorescence intensity $I(t) = \frac{I_b(t)}{I_c(t)}$. To investigate how composition and structure impact the fluidity of the overall membrane, we apply FRAP to a range of formulations, labeled F1 to F5, as listed in the table in Figure 4B. The normalized fluorescence intensity in a DOPC vesicle recovers to a plateau intensity, I_p, which is 100% of the unbleached control fluorescence, as shown by the blue curve in Figure 4C. As the polymer content increases to 20 wt% in vesicles, the fluorescence intensity takes longer to recover, reaching approximately 90%, as indicated by the purple curve in Figure 4C. We observe a similar prolonged recovery time when the polymer content increases

to 80 wt%, as shown by the green curve in Figure 4C. To examine lipid diffusion in asymmetric vesicles, we observe that vesicles with 66% asymmetry show fluorescence recovery to approximately 90%, with a time scale similar to vesicles composed of 80 wt% polymer, as depicted by the yellow curve in Figure 4C. As the degree of asymmetry increases to 78%, it takes significantly longer for the fluorescence to recover to approximately 70%, and full recovery extends beyond our experimental time window, as shown by the red curve in Figure 4C.

To determine whether the lipids are diffusing normally, we employ a semi-log plot to obtain $\log\left(I_p - I(t)\right)$ versus t for vesicles of different compositions, as shown in Figure 4D. We observe linear behaviors for all vesicles, indicating an exponential recovery consistent with normal diffusive behaviors for the lipids. Thus, we fit the normalized recovery fluorescence to $I(t) = I_o(1 - \exp\left(-\frac{t}{\tau_D}\right))$ (103). Using the intensity recovery plots in Figure 4C, we determine the half time, $\tau_{1/2} = -(\ln 0.5)\tau_D$, defined as the time it takes to recover to half of the plateau intensity.

To quantify how composition and structure affect the fluidity of membranes, we repeat the FRAP experiment with varying bleached areas, with bleached radius r , as illustrated by the schematic for a DOPC vesicle in Figure 4E, and obtain their half time of recovery dependent on bleached size. The larger the bleached area, the longer it takes for the lipids to diffuse into the bleached region. To explore lipid diffusivity in vesicles of different compositions and structures, we plot the bleached area size versus recovery half time for each vesicle type. We observe linear relationships between r^2 and $\tau_{1/2}$ for all vesicle types, as shown by Figure 4F. As we increase the polymer content from 0 wt% to 80 wt% in symmetric vesicles from F1 to F3, the lines exhibit decreasing slopes, indicated by the light blue, purple, and green lines in Figure 4F. This trend shows that the fluidity of the membrane decreases with increasing polymer content. To examine the effect of asymmetry on lipid diffusion, we study asymmetric vesicles with polymer inner and lipid outer leaflets, with a lower asymmetry degree of 66%, labeled F4. Interestingly, the intensity versus half time line approximately overlaps with that of symmetric vesicles with 80 wt% polymer, labeled F3, as shown by comparing the yellow line with the green line in Figure 4F. This result suggests that the polymer leaflet may be discontinuous in this type of asymmetric vesicle, resulting in a similar diffusion rate as in a high-polymer symmetric membrane. As we increase the degree of asymmetry from F4 to F5, we find that the slope decreases significantly, as indicated by comparing the green line with the red line in Figure 4F. This suggests that increasing asymmetry likely allows a continuous polymer leaflet, which slows lipid diffusion due to the large hydrophobic tails of the polymers.

To quantify the diffusion coefficients, D, we use the equation $D = \frac{r^2}{4\tau_{1/2}}$ (103), derived from the slope of the r^2 versus $4\tau_{1/2}$ line and summarize the statistics in Figure 4G (105). We plot the mean and standard deviation of the diffusion coefficients for all types of vesicles, as shown in Figure 4G. For DOPC vesicles, we determine the lipid diffusion coefficient to be approximately 6.1 $\mu m^2/s$, as shown by the light blue bar in Figure 4G. As polymer content increase to 20 wt% and 80 wt%, the diffusion coefficient drops approximately by 33% to 4.0 $\mu m^2/s$ and by 78% to 1.3 $\mu m^2/s$, as shown by the purple and green bars, respectively, in Figure 4G. For asymmetric vesicles with 66% asymmetry, the diffusion coefficient is 0.9 $\mu m^2/s$, which is slightly lower than that of the vesicles with 80 wt% polymers, as shown by the yellow bar in Figure 4G. By contrast, for vesicles with 78% asymmetry, the diffusion coefficient further decreases by another factor of 3 to approximately 0.2 $\mu m^2/s$, as indicated by the red bar in Figure 4G. This decrease in diffusion coefficient suggests that the polymers form a fully continuous leaflet in these highly asymmetric vesicles, drastically slowing the lipid diffusion.

Transmembrane Diffusion through Symmetric and Asymmetric Hybrid Vesicles Assessed by Fluorescence Imaging

To explore the effect of leaflet asymmetry on membrane permeability, we compare the influx rate of fluorescent dyes from the outer medium into the cores of different types of vesicles with identical radii (106-117). Specifically, we compare permeation rate for symmetric vesicles containing 80 wt% polymer, labeled F3, to asymmetric vesicles containing an assumed 50 wt% polymer and 78% asymmetry, labeled F5. We also include control groups using DOPC vesicles, labeled F1, and polymersomes, labeled F6, in our analysis. We examine their membrane permeation by adding 3000 Da FITC-dextran dye to the outer medium, as illustrated in Figure 5A. Immediately after adding the dye, we observe that the cores of the DOPC vesicles exhibit the same fluorescence as the outer medium, as indicated by the fluorescent image in the first row of Figure 5B. This observation demonstrates that

DOPC lipid leaflets are highly permeable to this dye. As we increase the polymer content to 80 wt% in symmetric vesicles, the fluorescence intensity in the core gradually increases over two hours until saturation, as shown by the fluorescent images in the second row of Figure 5B. This result indicates that increasing polymer content reduces permeability in symmetric vesicles. For asymmetric vesicles with 78% asymmetry and polymersomes, the fluorescence remains outside their cores for the entire 2-hour duration of the experiment, as shown by the images in the third and fourth rows of Figure 5B. This indicates that a single or double continuous polymer leaflet acts as an effective barrier to prevent membrane permeation.

To investigate the permeability of vesicles towards smaller molecules, we repeat the experiment using 300 Da fluorescein dye, as depicted in Figure 5C. We observe that the fluorescent dye diffuses into and saturates the DOPC vesicles, labeled F1, and symmetric vesicles with 80 wt% polymer, labeled F3, almost immediately, as shown by the first and second rows of Figure 5D, indicating their high permeability. In contrast, the asymmetric vesicles with lipid inner and polymer outer leaflets, labeled F4, are permeable to the dye, with their cores becoming fluorescently saturated after one hour, as shown by the third row in Figure 5D. Comparatively, polymersomes, labeled F5, of approximately the same diameter take about twice as long for the fluorescence to reach near saturation levels in the core, as shown by the fourth row in Figure 5D. Indeed, the fluorescent intensity in the cores of vesicles, normalized to the intensity in the medium, shows that the fluorescence increases approximately twice as fast in asymmetric vesicles as compared to polymersomes, as plotted in Figure 5E. We estimate the diffusion constant of dyes across the membrane, D_{eff}, from the slope of the fluorescence curve. We characterize the influx of molecules by $c_{in}(t) = c_{out}\left(1 - e^{-\frac{3D_{eff}}{Rl}t}\right)$, where c_{in} and c_{out} are concentrations of dyes inside and outside of the vesicle, R is the vesicle radius, and l is the pore length(106). Consequently, we characterize the linear regime in the fluorescence intensity versus time graph by $I_{in}(t) = \frac{c_{in}(t)}{c_{out}} = -\frac{3D_{eff}}{Rl}t$. Thus, for vesicles of identical radii, the diffusion constant is approximately twice as large in asymmetric vesicles compared to polymersomes. Since diffusion constant can be written as, $D_{eff} = Pd/K$ (117), where P is the intrinsic permeability coefficient of membranes, K is the oil/water partition coefficient, and d is the membrane thickness, the twice as large diffusion constant for the asymmetric vesicles suggests a thinner and more permeable membrane as compared to polymersomes, further corroborating a single continuous polymer leaflet in asymmetric vesicles. To demonstrate the potential usability by these asymmetric vesicles, we encapsulate fluorescently labelled doxorubicin, a model cancer drug, protonated by citric acid, inside these vesicles, as shown by the fluorescent image in the supplement. The lipid inner leaflet is biocompatible for many potential drugs, such as small molecules and proteins(2, 118-120), while the polymer outer leaflet protects the cargo from the harsh exterior environment.

Conclusion

In this work, we present a novel method to fabricate hybrid vesicles with engineered leaflet compositions and asymmetry. Our results show that a fully continuous polymer leaflet makes asymmetric hybrid vesicles significantly stiffer and tougher, with reduced fluidity and membrane pore size, as compared with symmetric hybrid vesicles. Leaflet asymmetry introduces a new degree of freedom to manipulate hybrid vesicles properties, expanding their potential applications in pharmaceuticals, biosensors, and artificial cells(12, 24, 81, 121-124), where precise control of vesicle properties is crucial.

Materials and Methods

Chemicals. We use 1,2-dioleyl-sn-glycero-3-phosphocholine (DOPC), 1,2-dioleoyl-sn-glycero-3-phosphoethanolamine-N-(lissamine rhodamine B sulfonyl) (ammonium salt) (DOPE-Rodamine), 1,2-dioleoyl-sn-glycero-3-phosphoethanolamine-N-(7-nitro-2-1,3-benzoxadiazol-4-yl) (ammonium salt)(DOPE-NBD), and 1,2-dioleoyl-sn-glycero-3-phosphoethanolamine-N-(carboxyfluorescein) (ammonium salt) (DOPE-carboxy fluorescein), purchased from Avanti Polar Lipids Inc. The polymer, 10kDa Poly(ethylene glycol)-block- 15kDa poly(D,L-lactic acid) (PEG-b-PLA) and fluorescein isothiocyanate-10kDa PEG-b-15kDa PLA (FITC-10kDa PEG-b-15kDa PLA) are purchased from Polysciences Inc and Nanosoftpolymers Inc respectively. We purchase 6000Da Poly(ethylene glycol) (PEG), poly(vinyl alcohol) (PVA, 13 – 23 KDa, 87-89 % hydrolyzed), hexane, and chloroform all from Sigma. The phosphate buffered saline (PBS) solution is purchased from ThermoFisher Scientific.

Glass Capillary Device Fabrication. We use square borosilicate glass capillaries with

Internal diameter 1.05 mm purchased from Atlantic International Technology and round borosilicate glass capillaries with external diameter 1.00 mm and internal diameter 0.58 mm purchased from World Precision Instruments. Both square and round capillaries are tapered using a micropipette puller (P-97, Sutter Instrument, Inc.) and sanded using a sand paper (2500 grit) to adjust the final diameters of the capillary openings. We purchase the hydrophobic coating, trimethoxy(octadecyl) silane purchased from Sigma and the hydrophilibc coating, 2-[methoxy(polyethyleneoxy)9-12propyl] trimethoxysilane, purchased from Gelest. Additional smaller round capillaries are made by stretching a round capillary over a burner. We align the device under a microscope and use 5 min epoxy (Devcon) to bound the device to a glass slide. Needles with inner connections (0.5" needle length, 20 gauge) are purchased from McMaster-Carr and glued at the capillary openings where we introduce fluids.

Microfluidic Fabrication. A range of chemical compositions work for making symmetric and asymmetric hybrid vesicles using a microfluidic device. Symmetric hybrid vesicles have been made using 5-10 mg/ml of mixed lipids and polymer in a chloroform and hexane mixture. Chloroform to hexane volume ratio from 1:1.6 to 1:1.8 work depending on the quality of the lipid and polymer. The lipids and polymers should be used within 1-2 weeks upon arrival. Asymmetric hybrid vesicles have been made with 10-18 mg/ml of separately dissolved lipids and polymer in two different chloroform and hexane mixtures. We have also tested using lipids at a lower concentration, such as 10 mg/ml, and polymers at a higher concentration, such as 18 mg/ml. The imbalanced ratio can potentially introduce more polymer into the asymmetric vesicles and enhance asymmetry. Supplementary videos V1 and V2 showing production of symmetric and asymmetric vesicles are available.

Micropipette Aspiration. During the aspiration, we record the optical images of vesicles into a video and the incremental pressure into an excel file using the software Oxygen linked to a negative pressure controller with range between 0 mbar to 25 mbar purchased from Fluigent Inc. We analyze the images using MATLAB, and obtain the areal strain (α) using $\alpha = \frac{\Delta A}{A_o} = \frac{2\pi R_p L}{A_o}(1 - \frac{R_p}{R_s})$, where L is the length of the projected membrane inside the pipette, A_o is the original spherical surface area of the vesicle, and R_p and R_s are the radii of the pipette and the outer radius of the vesicles respectively. We also use MATLAB to calculate the membrane tension from the pressure data. Supplementary videos V3 and V4 showing aspiration are available.

FRAP. We use the FRAP module within the Leica SP5 confocal software. We bleach the vesicles for 1-10 seconds depending on the size of the bleached spot, and acquire the images every 0.5s to 60s depending on the total time needed for the recovery to avoid excessive additional bleaching of the fluorophore during the image acquisition. The measured intensities are normalized to the prebleach intensities of the region of interest (ROI), and a control ROI helps adjust for the bleaching of the sample during image acquisition. We observe the fluorescence intensity virtually recovers to the prebleached intensity. Thus, we simplify the normalized intensity recovery fitting to $I(t) = \mathrm{A} \times (1 - \exp(-\frac{t}{\tau_D}))$. Supplementary video of an asymmetric vesicle during FRAP experiment is available.

Supplement

Supplementary files and videos are available.

Acknowledgement

This work is based on support by the Harvard MRSEC funding DMR-2011754 and the Health@InnoHK program of the Innovation and Technology Commission of the Hong Kong SAR Government. We thank our funding sources for enabling us to do these experiments.

1. Chacko IA, Ghate VM, Dsouza L, Lewis SA. Lipid vesicles: A versatile drug delivery platform for dermal and transdermal applications. Colloids and Surfaces B: Biointerfaces. 2020;195:111262.
2. Jain S, Jain V, Mahajan S. Lipid based vesicular drug delivery systems. Advances in Pharmaceutics. 2014;2014(1):574673.
3. van der Meel R, Fens MH, Vader P, Van Solinge WW, Eniola-Adefeso O, Schiffelers RM. Extracellular vesicles as drug delivery systems: lessons from the liposome field. Journal of controlled release. 2014;195:72-85.
4. Zhang L, Chan JM, Gu FX, Rhee J-W, Wang AZ, Radovic-Moreno AF, et al. Self-assembled lipid–polymer hybrid nanoparticles: a robust drug delivery platform. ACS nano. 2008;2(8):1696-702.
5. Kauscher U, Holme MN, Björnmalm M, Stevens MM. Physical stimuli-responsive vesicles in drug delivery: Beyond liposomes and polymersomes. Advanced drug delivery reviews. 2019;138:259-75.
6. Pautot S, Frisken BJ, Weitz D. Engineering asymmetric vesicles. Proceedings of the National Academy of Sciences. 2003;100(19):10718-21.
7. Miatmoko A, Ayunin Q, Soeratri W. Ultradeformable vesicles: concepts and applications relating to the delivery of skin cosmetics. Therapeutic Delivery. 2021;12(10):739-56.
8. Reiner AT, Somoza V. Extracellular vesicles as vehicles for the delivery of food bioactives. Journal of agricultural and food chemistry. 2019;67(8):2113-9.
9. Kang JY, Choi I, Seo M, Lee JY, Hong S, Gong G, et al. Enhancing membrane modulus of giant unilamellar lipid vesicles by lateral co-assembly of amphiphilic triblock copolymers. Journal of colloid and interface science. 2020;561:318-26.
10. Chemin M, Brun P-M, Lecommandoux S, Sandre O, Le Meins J-F. Hybrid polymer/lipid vesicles: fine control of the lipid and polymer distribution in the binary membrane. Soft Matter. 2012;8(10):2867-74.
11. Le Meins J-F, Schatz C, Lecommandoux S, Sandre O. Hybrid polymer/lipid vesicles: state of the art and future perspectives. Materials today. 2013;16(10):397-402.
12. Go YK, Leal C. Polymer–lipid hybrid materials. Chemical reviews. 2021;121(22):13996-4030.
13. Discher DE, Ahmed F. Polymersomes. Annu Rev Biomed Eng. 2006;8(1):323-41.
14. Rideau E, Dimova R, Schwille P, Wurm FR, Landfester K. Liposomes and polymersomes: a comparative review towards cell mimicking. Chemical society reviews. 2018;47(23):8572-610.
15. Discher BM, Won Y-Y, Ege DS, Lee JC, Bates FS, Discher DE, et al. Polymersomes: tough vesicles made from diblock copolymers. Science. 1999;284(5417):1143-6.
16. Chang H-Y, Sheng Y-J, Tsao H-K. Structural and mechanical characteristics of polymersomes. Soft Matter. 2014;10(34):6373-81.
17. Discher BM, Bermudez H, Hammer DA, Discher DE, Won Y-Y, Bates FS. Cross-linked polymersome membranes: vesicles with broadly adjustable properties. The Journal of Physical Chemistry B. 2002;106(11):2848-54.
18. Matoori S, Leroux J-C. Twenty-five years of polymersomes: lost in translation? Materials Horizons. 2020;7(5):1297-309.
19. Schulz M, Binder WH. Mixed hybrid lipid/polymer vesicles as a novel membrane platform. Macromolecular rapid communications. 2015;36(23):2031-41.
20. Fauquignon M, Ibarboure E, Le Meins J-F. Membrane reinforcement in giant hybrid polymer lipid vesicles achieved by controlling the polymer architecture. Soft Matter. 2021;17(1):83-9.

21. Fauquignon M, Courtecuisse E, Josselin R, Mutschler A, Brûlet A, Schmutz M, et al. Large hybrid Polymer/Lipid Unilamellar vesicle (LHUV) at the nanoscale: An insight into the lipid distribution in the membrane and permeability control. Journal of Colloid and Interface Science. 2021;604:575-83.
22. Hamada N, Gakhar S, Longo ML. Hybrid lipid/block copolymer vesicles display broad phase coexistence region. Biochimica et Biophysica Acta (BBA)-Biomembranes. 2021;1863(4):183552.
23. Perrotton J, Ahijado-Guzmán R, Moleiro LH, Tinao B, Guerrero-Martinez A, Amstad E, et al. Microfluidic fabrication of vesicles with hybrid lipid/nanoparticle bilayer membranes. Soft Matter. 2019;15(6):1388-95.
24. Mohammadi M, Taghavi S, Abnous K, Taghdisi SM, Ramezani M, Alibolandi M. Hybrid vesicular drug delivery systems for cancer therapeutics. Advanced Functional Materials. 2018;28(36):1802136.
25. Schulz M, Glatte D, Meister A, Scholtysek P, Kerth A, Blume A, et al. Hybrid lipid/polymer giant unilamellar vesicles: effects of incorporated biocompatible PIB–PEO block copolymers on vesicle properties. Soft Matter. 2011;7(18):8100-10.
26. Meyer CE, Abram S-L, Craciun I, Palivan CG. Biomolecule–polymer hybrid compartments: combining the best of both worlds. Physical Chemistry Chemical Physics. 2020;22(20):11197-218.
27. Hu S-W, Huang C-Y, Tsao H-K, Sheng Y-J. Hybrid membranes of lipids and diblock copolymers: From homogeneity to rafts to phase separation. Physical Review E. 2019;99(1):012403.
28. Magnani C, Montis C, Mangiapia G, Mingotaud A-F, Mingotaud C, Roux C, et al. Hybrid vesicles from lipids and block copolymers: Phase behavior from the micro-to the nano-scale. Colloids and Surfaces B: Biointerfaces. 2018;168:18-28.
29. Marušič N, Otrin L, Rauchhaus J, Zhao Z, Kyrilis FL, Hamdi F, et al. Increased efficiency of charge-mediated fusion in polymer/lipid hybrid membranes. Proceedings of the National Academy of Sciences. 2022;119(20):e2122468119.
30. Zhang H, Cui W, Qu X, Wu H, Qu L, Zhang X, et al. Photothermal-responsive nanosized hybrid polymersome as versatile therapeutics codelivery nanovehicle for effective tumor suppression. Proceedings of the National Academy of Sciences. 2019;116(16):7744-9.
31. Yadavalli SS, Xiao Q, Sherman SE, Hasley WD, Klein ML, Goulian M, et al. Bioactive cell-like hybrids from dendrimersomes with a human cell membrane and its components. Proceedings of the National Academy of Sciences. 2019;116(3):744-52.
32. Taubert A. Controlling water transport through artificial polymer/protein hybrid membranes. Proceedings of the National Academy of Sciences. 2007;104(52):20643-4.
33. Beales PA, Khan S, Muench SP, Jeuken LJ. Durable vesicles for reconstitution of membrane proteins in biotechnology. Biochemical Society Transactions. 2017;45(1):15-26.
34. Jacobs ML, Boyd MA, Kamat NP. Diblock copolymers enhance folding of a mechanosensitive membrane protein during cell-free expression. Proceedings of the national academy of sciences. 2019;116(10):4031-6.
35. Gispert I, Hindley JW, Pilkington CP, Shree H, Barter LM, Ces O, et al. Stimuli-responsive vesicles as distributed artificial organelles for bacterial activation. Proceedings of the National Academy of Sciences. 2022;119(42):e2206563119.
36. Müller WA, Beales PA, Muniz AR, Jeuken LJ. Unraveling the Phase Behavior, Mechanical Stability, and Protein Reconstitution Properties of Polymer–Lipid Hybrid Vesicles. Biomacromolecules. 2023;24(9):4156-69.

37. Winzen S, Bernhardt M, Schaeffel D, Koch A, Kappl M, Koynov K, et al. Submicron hybrid vesicles consisting of polymer–lipid and polymer–cholesterol blends. Soft Matter. 2013;9(25):5883-90.
38. Huang C, Quinn D, Sadovsky Y, Suresh S, Hsia KJ. Formation and size distribution of self-assembled vesicles. Proceedings of the National Academy of Sciences. 2017;114(11):2910-5.
39. Fauquignon M, Ibarboure E, Le Meins J-F. Hybrid polymer/lipid vesicles: Influence of polymer architecture and molar mass on line tension. Biophysical Journal. 2022;121(1):61-7.
40. Jahnke K, Pavlovic M, Xu W, Chen A, Knowles TP, Arriaga LR, et al. Polysaccharide functionalization reduces lipid vesicle stiffness. Proceedings of the National Academy of Sciences. 2024;121(22):e2317227121.
41. Henderson IM, Paxton WF. Salt, shake, fuse—giant hybrid polymer/lipid vesicles through mechanically activated fusion. Angewandte Chemie. 2014;126(13):3440-4.
42. Lira RB, Dimova R, Riske KA. Giant unilamellar vesicles formed by hybrid films of agarose and lipids display altered mechanical properties. Biophysical journal. 2014;107(7):1609-19.
43. Nam J, Beales PA, Vanderlick TK. Giant phospholipid/block copolymer hybrid vesicles: Mixing behavior and domain formation. Langmuir. 2011;27(1):1-6.
44. Chen D, Santore MM. Hybrid copolymer–phospholipid vesicles: phase separation resembling mixed phospholipid lamellae, but with mechanical stability and control. Soft Matter. 2015;11(13):2617-26.
45. Richmond DL, Schmid EM, Martens S, Stachowiak JC, Liska N, Fletcher DA. Forming giant vesicles with controlled membrane composition, asymmetry, and contents. Proceedings of the National Academy of Sciences. 2011;108(23):9431-6.
46. Krompers M, Heerklotz H. A guide to your desired lipid-asymmetric vesicles. Membranes. 2023;13(3):267.
47. Peyret A, Zhao H, Lecommandoux S. Preparation and properties of asymmetric synthetic membranes based on lipid and polymer self-assembly. Langmuir. 2018;34(11):3376-85.
48. Tsai H-C, Yang Y-L, Sheng Y-J, Tsao H-K. Formation of asymmetric and symmetric hybrid membranes of lipids and triblock copolymers. Polymers. 2020;12(3):639.
49. Peyret A, Ibarboure E, Le Meins JF, Lecommandoux S. Asymmetric hybrid polymer–lipid giant vesicles as cell membrane mimics. Advanced Science. 2018;5(1):1700453.
50. Arriaga LR, Huang Y, Kim S-H, Aragones JL, Ziblat R, Koehler SA, et al. Single-step assembly of asymmetric vesicles. Lab on a Chip. 2019;19(5):749-56.
51. Wen L, Xiao K, Sainath AVS, Komura M, Kong XY, Xie G, et al. Engineered asymmetric composite membranes with rectifying properties. Advanced Materials. 2016;28(4):757-63.
52. Yu H, Qiu X, Moreno N, Ma Z, Calo VM, Nunes SP, et al. Self-assembled asymmetric block copolymer membranes: bridging the gap from ultra-to nanofiltration. Angewandte Chemie. 2015;127(47):14143-7.
53. Pabst G, Keller S. Exploring membrane asymmetry and its effects on membrane proteins. Trends in Biochemical Sciences. 2024.
54. Zhang Z, Kong X-Y, Xiao K, Liu Q, Xie G, Li P, et al. Engineered asymmetric heterogeneous membrane: a concentration-gradient-driven energy harvesting device. Journal of the American Chemical Society. 2015;137(46):14765-72.
55. Zhang Z, Wen L, Jiang L. Bioinspired smart asymmetric nanochannel membranes. Chemical Society Reviews. 2018;47(2):322-56.

56. Bretscher MS. Membrane Structure: Some General Principles: Membranes are asymmetric lipid bilayers in which cytoplasmically synthesized proteins are· dissolved. Science. 1973;181(4100):622-9.
57. Lorent J, Levental KR, Ganesan L, Rivera-Longsworth G, Sezgin E, Doktorova M, et al. Plasma membranes are asymmetric in lipid unsaturation, packing and protein shape. Nature chemical biology. 2020;16(6):644-52.
58. Doktorova M, Symons JL, Levental I. Structural and functional consequences of reversible lipid asymmetry in living membranes. Nature chemical biology. 2020;16(12):1321-30.
59. London E. Membrane structure–function insights from asymmetric lipid vesicles. Accounts of chemical research. 2019;52(8):2382-91.
60. Kamiya K, Kawano R, Osaki T, Akiyoshi K, Takeuchi S. Cell-sized asymmetric lipid vesicles facilitate the investigation of asymmetric membranes. Nature chemistry. 2016;8(9):881-9.
61. Low W-Y, Thong S, Chng S-S. ATP disrupts lipid-binding equilibrium to drive retrograde transport critical for bacterial outer membrane asymmetry. Proceedings of the National Academy of Sciences. 2021;118(50):e2110055118.
62. Powers MJ, Trent MS. Phospholipid retention in the absence of asymmetry strengthens the outer membrane permeability barrier to last-resort antibiotics. Proceedings of the National Academy of Sciences. 2018;115(36):E8518-E27.
63. Henderson JC, Zimmerman SM, Crofts AA, Boll JM, Kuhns LG, Herrera CM, et al. The power of asymmetry: architecture and assembly of the Gram-negative outer membrane lipid bilayer. Annual review of microbiology. 2016;70(1):255-78.
64. Guest RL, Lee MJ, Wang W, Silhavy TJ. A periplasmic phospholipase that maintains outer membrane lipid asymmetry in Pseudomonas aeruginosa. Proceedings of the National Academy of Sciences. 2023;120(30):e2302546120.
65. Arriaga LR, Datta SS, Kim SH, Amstad E, Kodger TE, Monroy F, et al. Ultrathin shell double emulsion templated giant unilamellar lipid vesicles with controlled microdomain formation. small. 2014;10(5):950-6.
66. do Nascimento DbF, Arriaga LR, Eggersdorfer M, Ziblat R, Marques MdFV, Reynaud F, et al. Microfluidic fabrication of pluronic vesicles with controlled permeability. Langmuir. 2016;32(21):5350-5.
67. Kim S-H, Shum HC, Kim JW, Cho J-C, Weitz DA. Multiple polymersomes for programmed release of multiple components. Journal of the American Chemical Society. 2011;133(38):15165-71.
68. Qian W, Song X, Feng C, Xu P, Jiang X, Li Y, et al. Construction of PEG-based amphiphilic brush polymers bearing hydrophobic poly (lactic acid) side chains via successive RAFT polymerization and ROP. Polymer Chemistry. 2016;7(19):3300-10.
69. Li T, Zhang J, Schneiderman DK, Francis LF, Bates FS. Toughening glassy poly (lactide) with block copolymer micelles. ACS Macro Letters. 2016;5(3):359-64.
70. Grundler J, Shin K, Suh H-W, Zhong M, Saltzman WM. Surface topography of polyethylene glycol shell nanoparticles formed from bottlebrush block copolymers controls interactions with proteins and cells. ACS nano. 2021;15(10):16118-29.
71. Pagels RF, Edelstein J, Tang C, Prud'homme RK. Controlling and predicting nanoparticle formation by block copolymer directed rapid precipitations. Nano Letters. 2018;18(2):1139-44.
72. Oh JK. Polylactide (PLA)-based amphiphilic block copolymers: synthesis, self-assembly, and biomedical applications. Soft Matter. 2011;7(11):5096-108.
73. Kutikov AB, Song J. Biodegradable PEG-based amphiphilic block copolymers for tissue engineering applications. ACS biomaterials science & engineering. 2015;1(7):463-80.

74. Qi H, Zhou H, Tang Q, Lee JY, Fan Z, Kim S, et al. Block copolymer crystalsomes with an ultrathin shell to extend blood circulation time. Nature communications. 2018;9(1):3005.
75. Kwon Y, Kim KT. Crystallization-driven self-assembly of block copolymers having monodisperse poly (lactic acid) s with defined stereochemical sequences. Macromolecules. 2021;54(22):10487-98.
76. Gambin Y, Lopez-Esparza R, Reffay M, Sierecki E, Gov N, Genest M, et al. Lateral mobility of proteins in liquid membranes revisited. Proceedings of the National Academy of Sciences. 2006;103(7):2098-102.
77. Espinosa G, López-Montero I, Monroy F, Langevin D. Shear rheology of lipid monolayers and insights on membrane fluidity. Proceedings of the National Academy of Sciences. 2011;108(15):6008-13.
78. Chen D, Santore MM. Large effect of membrane tension on the fluid–solid phase transitions of two-component phosphatidylcholine vesicles. Proceedings of the national academy of sciences. 2014;111(1):179-84.
79. Sivars U, Tjerneld F. Mechanisms of phase behaviour and protein partitioning in detergent/polymer aqueous two-phase systems for purification of integral membrane proteins. Biochimica et Biophysica Acta (BBA)-General Subjects. 2000;1474(2):133-46.
80. Marconnet A, Michon B, Le Bon C, Giusti F, Tribet C, Zoonens M. Solubilization and stabilization of membrane proteins by cycloalkane-modified amphiphilic polymers. Biomacromolecules. 2020;21(8):3459-67.
81. Pocanschi CL, Dahmane T, Gohon Y, Rappaport F, Apell H-J, Kleinschmidt JH, et al. Amphipathic polymers: tools to fold integral membrane proteins to their active form. Biochemistry. 2006;45(47):13954-61.
82. Itel F, Najer A, Palivan CG, Meier W. Dynamics of membrane proteins within synthetic polymer membranes with large hydrophobic mismatch. Nano letters. 2015;15(6):3871-8.
83. Angeletti C, Nichols JW. Dithionite quenching rate measurement of the inside− outside membrane bilayer distribution of 7-nitrobenz-2-oxa-1, 3-diazol-4-yl-labeled phospholipids. Biochemistry. 1998;37(43):15114-9.
84. Gomišček G, Arrigler V, Gros M, Zupančič M, Svetina S. Asymmetrical labeling of giant phospholipid vesicles. Pflügers Archiv-European Journal of Physiology. 2000;440:R051-R2.
85. McIntyre JC, Sleight RG. Fluorescence assay for phospholipid membrane asymmetry. Biochemistry. 1991;30(51):11819-27.
86. Henriksen JR, Ipsen JH. Measurement of membrane elasticity by micro-pipette aspiration. The European physical journal E. 2004;14:149-67.
87. Vaziri A, Mofrad MRK. Mechanics and deformation of the nucleus in micropipette aspiration experiment. Journal of biomechanics. 2007;40(9):2053-62.
88. Rawicz W, Olbrich KC, McIntosh T, Needham D, Evans E. Effect of chain length and unsaturation on elasticity of lipid bilayers. Biophysical journal. 2000;79(1):328-39.
89. Dasgupta R, Miettinen MS, Fricke N, Lipowsky R, Dimova R. The glycolipid GM1 reshapes asymmetric biomembranes and giant vesicles by curvature generation. Proceedings of the National Academy of Sciences. 2018;115(22):5756-61.
90. Guevorkian K, Gonzalez-Rodriguez D, Carlier C, Dufour S, Brochard-Wyart F. Mechanosensitive shivering of model tissues under controlled aspiration. Proceedings of the National Academy of Sciences. 2011;108(33):13387-92.

91. Di Cerbo A, Rubino V, Morelli F, Ruggiero G, Landi R, Guidetti G, et al. Mechanical phenotyping of K562 cells by the Micropipette Aspiration Technique allows identifying mechanical changes induced by drugs. Scientific reports. 2018;8(1):1219.
92. Brugués J, Maugis B, Casademunt J, Nassoy P, Amblard F, Sens P. Dynamical organization of the cytoskeletal cortex probed by micropipette aspiration. Proceedings of the National Academy of Sciences. 2010;107(35):15415-20.
93. Guevorkian K, Maître J-L. Micropipette aspiration: A unique tool for exploring cell and tissue mechanics in vivo. Methods in cell biology. 139: Elsevier; 2017. p. 187-201.
94. Lee LM, Liu AP. The application of micropipette aspiration in molecular mechanics of single cells. Journal of nanotechnology in engineering and medicine. 2014;5(4):040902.
95. González-Bermúdez B, Guinea GV, Plaza GR. Advances in micropipette aspiration: applications in cell biomechanics, models, and extended studies. Biophysical Journal. 2019;116(4):587-94.
96. Hochmuth RM. Micropipette aspiration of living cells. Journal of biomechanics. 2000;33(1):15-22.
97. Hsu C-P, Aretz J, Hordeichyk A, Fässler R, Bausch AR. Surface-induced phase separation of reconstituted nascent integrin clusters on lipid membranes. Proceedings of the National Academy of Sciences. 2023;120(31):e2301881120.
98. Solon J, Streicher P, Richter R, Brochard-Wyart F, Bassereau P. Vesicles surfing on a lipid bilayer: Self-induced haptotactic motion. Proceedings of the National Academy of Sciences. 2006;103(33):12382-7.
99. Cho N-J, Hwang LY, Solandt JJ, Frank CW. Comparison of extruded and sonicated vesicles for planar bilayer self-assembly. Materials. 2013;6(8):3294-308.
100. Dimova R. Giant vesicles and their use in assays for assessing membrane phase state, curvature, mechanics, and electrical properties. Annual review of biophysics. 2019;48(1):93-119.
101. Roder F, Waichman S, Paterok D, Schubert R, Richter C, Liedberg B, et al. Reconstitution of membrane proteins into polymer-supported membranes for probing diffusion and interactions by single molecule techniques. Analytical chemistry. 2011;83(17):6792-9.
102. Pace H, Simonsson Nyström L, Gunnarsson A, Eck E, Monson C, Geschwindner S, et al. Preserved transmembrane protein mobility in polymer-supported lipid bilayers derived from cell membranes. Analytical chemistry. 2015;87(18):9194-203.
103. Pincet F, Adrien V, Yang R, Delacotte J, Rothman JE, Urbach W, et al. FRAP to characterize molecular diffusion and interaction in various membrane environments. PloS one. 2016;11(7):e0158457.
104. Chattopadhyay M, Krok E, Orlikowska H, Schwille P, Franquelim HG, Piatkowski L. Hydration layer of only a few molecules controls lipid mobility in biomimetic membranes. Journal of the American Chemical Society. 2021;143(36):14551-62.
105. Kang M, Day CA, Kenworthy AK, DiBenedetto E. Simplified equation to extract diffusion coefficients from confocal FRAP data. Traffic. 2012;13(12):1589-600.
106. Fragasso A, De Franceschi N, Stömmer P, Van Der Sluis EO, Dietz H, Dekker C. Reconstitution of ultrawide DNA origami pores in liposomes for transmembrane transport of macromolecules. ACS nano. 2021;15(8):12768-79.
107. Leite NB, Aufderhorst-Roberts A, Palma MS, Connell SD, Neto JR, Beales PA. PE and PS lipids synergistically enhance membrane poration by a peptide with anticancer properties. Biophysical Journal. 2015;109(5):936-47.

108. Finkelstein A, Cass A. Permeability and electrical properties of thin lipid membranes. The Journal of general physiology. 1968;52(1):145-72.
109. Hanai T, Haydon D. The permeability to water of bimolecular lipid membranes. Journal of Theoretical Biology. 1966;11(3):370-82.
110. Seo PR, Teksin ZS, Kao JP, Polli JE. Lipid composition effect on permeability across PAMPA. European journal of pharmaceutical sciences. 2006;29(3-4):259-68.
111. Finkelstein A. Water and nonelectrolyte permeability of lipid bilayer membranes. The Journal of general physiology. 1976;68(2):127-35.
112. Gallucci E, Micelli S, Lippe C. Non-electrolyte permeability across thin lipid membranes. Archives Internationales de Physiologie et de Biochimie. 1971;79(5):881-7.
113. Mathai JC, Tristram-Nagle S, Nagle JF, Zeidel ML. Structural determinants of water permeability through the lipid membrane. The Journal of general physiology. 2008;131(1):69-76.
114. Marsh D. Polarity and permeation profiles in lipid membranes. Proceedings of the National Academy of Sciences. 2001;98(14):7777-82.
115. Cass A, Finkelstein A. Water permeability of thin lipid membranes. The Journal of general physiology. 1967;50(6):1765-84.
116. Fettiplace R, Haydon D. Water permeability of lipid membranes. Physiological Reviews. 1980;60(2):510-50.
117. Shinoda W. Permeability across lipid membranes. Biochimica et Biophysica Acta (BBA)-Biomembranes. 2016;1858(10):2254-65.
118. Guo X, Szoka FC. Chemical approaches to triggerable lipid vesicles for drug and gene delivery. Accounts of chemical research. 2003;36(5):335-41.
119. Xu X, Costa A, Burgess DJ. Protein encapsulation in unilamellar liposomes: high encapsulation efficiency and a novel technique to assess lipid-protein interaction. Pharmaceutical research. 2012;29:1919-31.
120. Tan Y-C, Hettiarachchi K, Siu M, Pan Y-R, Lee AP. Controlled microfluidic encapsulation of cells, proteins, and microbeads in lipid vesicles. Journal of the American Chemical Society. 2006;128(17):5656-8.
121. Xiao Q, Yadavalli SS, Zhang S, Sherman SE, Fiorin E, Da Silva L, et al. Bioactive cell-like hybrids coassembled from (glyco) dendrimersomes with bacterial membranes. Proceedings of the National Academy of Sciences. 2016;113(9):E1134-E41.
122. Krywko-Cendrowska A, Di Leone S, Bina M, Yorulmaz-Avsar S, Palivan CG, Meier W. Recent advances in hybrid biomimetic polymer-based films: from assembly to applications. Polymers. 2020;12(5):1003.
123. Lu Y, Allegri G, Huskens J. Vesicle-based artificial cells: materials, construction methods and applications. Materials horizons. 2022;9(3):892-907.
124. Trantidou T, Dekker L, Polizzi K, Ces O, Elani Y. Functionalizing cell-mimetic giant vesicles with encapsulated bacterial biosensors. Interface Focus. 2018;8(5):20180024.

Figures and Tables

Figure 1.

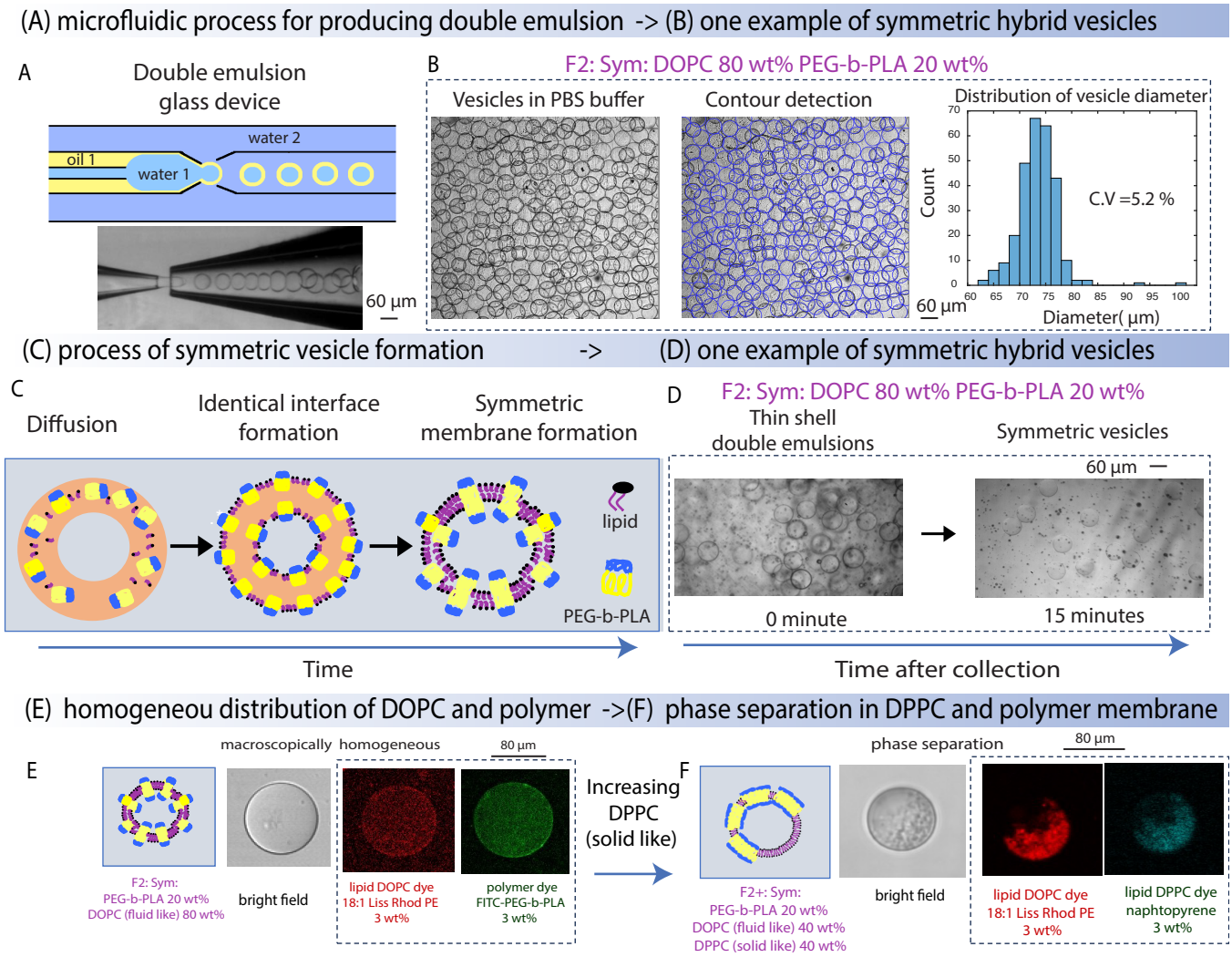

Figure 1. (A) (top) schematic illustration of the microfluidic device used to produce water-in-oil-in-water double emulsion drops and (bottom) optical microscope images showing the production of uniform double emulsions. (B) an exemplar sample, containing 80 wt% DOPC and 20 wt% PEG-b-PLA, with C.V analysis by image processing analysis from MATLAB. The first image is the bright filed image of sample; the second image detects all the vesicle contours; the third image plots the distribution of their diameters and calculates the C.V to be 5.2%, which is within the uniform vesicle range. (C) Schematic illustrating the transformation of double emulsions into symmetric polymer-lipid vesicles. (D) Optical microscope images of double emulsions transforming into vesicles where the thin oil shells leave and become thin membranes. (E) Fluorescence images of vesicles labelled with (right two) 3 wt% 18:1 Liss Rhod PE, the lipophilic dye, and (right one) 3 wt% FITC-PEG-b-PLA, the polymer dye. The lipids and polymers are distributed throughout the membrane. (F) Fluorescence images of vesicles labelled with (right two) 3 wt% 18:1 Liss Rhod PE, the DOPC affinity dye, and (right one) 3 wt% naphtopyrene, the DPPC affinity dye. The lipids, DOPC and DPPC, form a lipid rich region (red and blue), separates from the polymer rich region, which is non-fluorescent.

<insert page break here>

Figure 2.

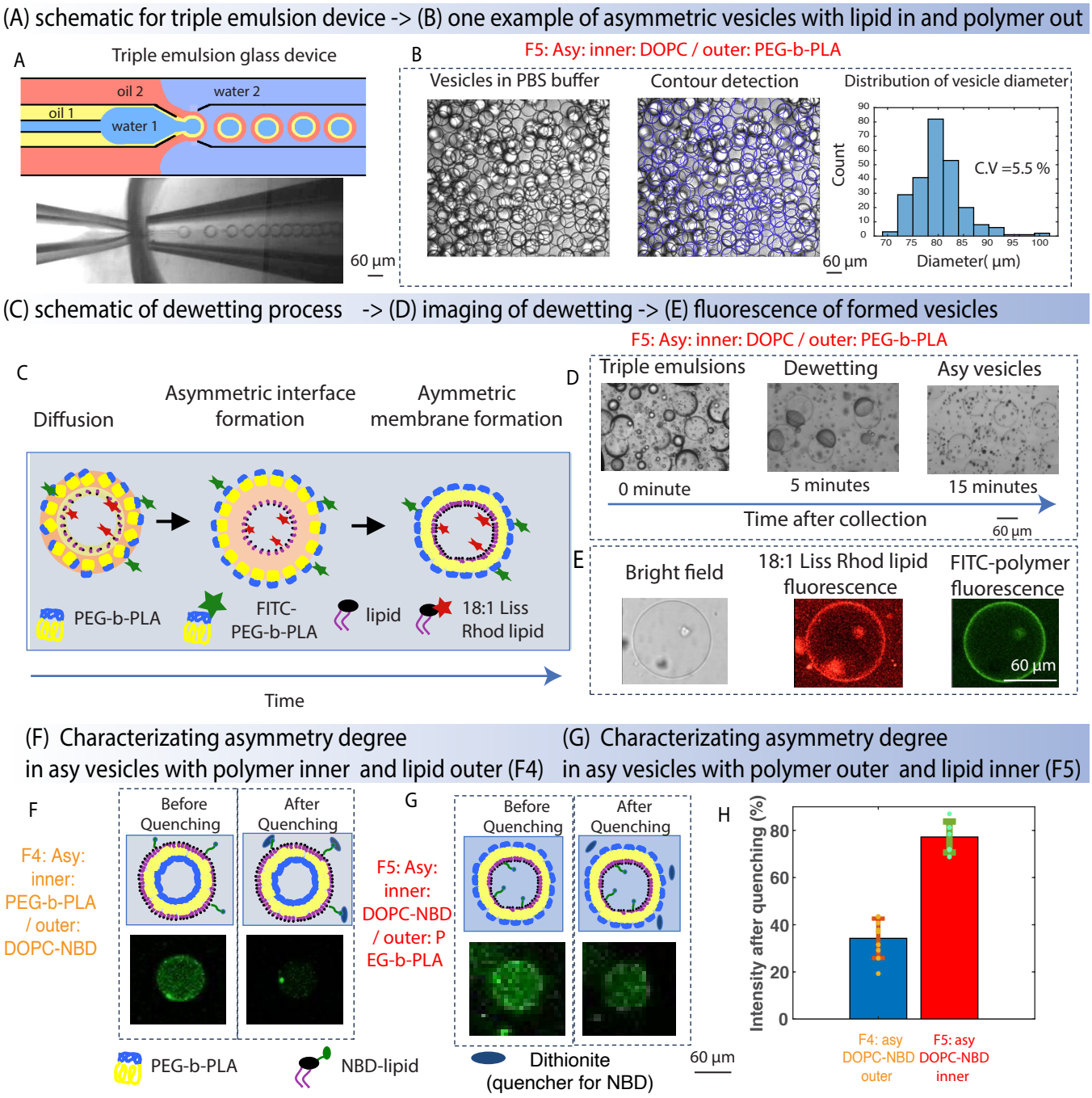

Figure 2. (A) (Left) schematic illustration of the microfluidic device used to produce water-in-oil-in-oil-in-water triple emulsion drops and (right) optical microscope images showing the production of uniform emulsions. (C) Schematic illustrating the transformation of triple emulsions into asymmetric polymer-lipid vesicles. (D) Optical microscope images of triple emulsions transforming into vesicles as the oil, which appears dark, leaves the vesicle membranes. (E) (F) Quenching the fluorescence in asymmetric vesicles. In the asymmetric vesicle with polymer inner and lipid outer as shown in the right images, the outer lipid leaflet is labeled with 3% NBD-DOPE, the fluorescent dye; upon addition of dithionite, the outer leaflet is exposed to the quencher, allowing its fluorescence to get quenched dramatically as compared to its original intensity. (G) In the asymmetric vesicle with polymer outer and lipid inner as shown in the left images, the inner lipid leaflet is labeled with 3 wt% NBD-DOPE; upon the addition of dithionite, the inner lipid lipid is shielded from the quencher, while the outer polymer rich leaflet, which may contain some lipid

contents, is exposed to the quencher. Its fluorescence gets quenched rmore slighlty as compared to the drop in fluorescence in (F), showing that most lipids ar in the inner leaflet, affirming asymmety. (H)Statistics of quenching from 4-6 vesicles from F4 and F5 samples. The results show that the asy vesicles with lipid outer are 66% asymmetric on average, while the asy vesicles with polymer outside show that the vesicle membranes are 75% asymmetric. The statistics show that F5 is more asymmetric than F4.

Figure 3

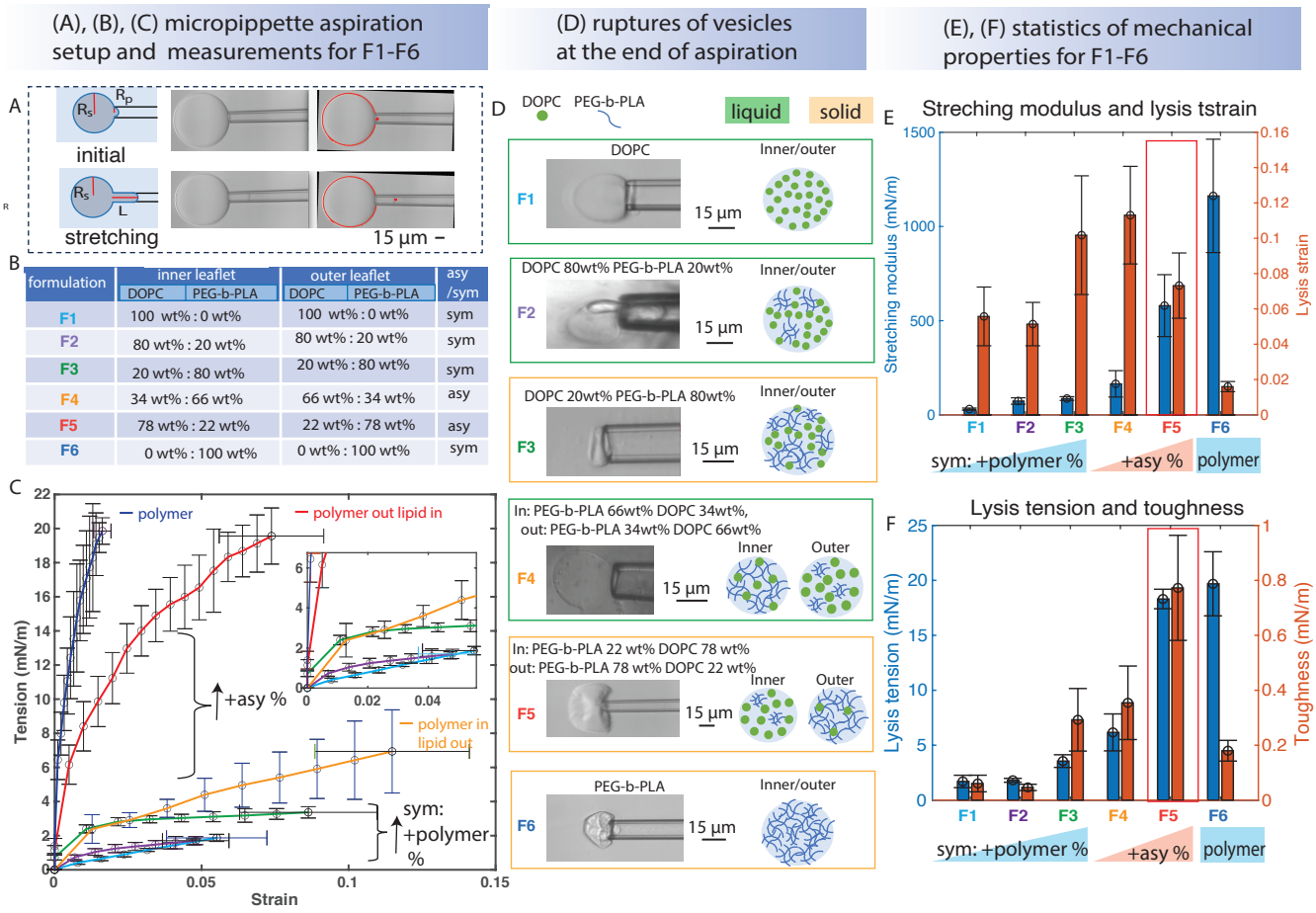

formulation	inner leaflet		outer leaflet		asy /sym
	DOPC	PEG-b-PLA	DOPC	PEG-b-PLA	
F1	100 wt% : 0 wt%		100 wt% : 0 wt%		sym
F2	80 wt% : 20 wt%		80 wt% : 20 wt%		sym
F3	20 wt% : 80 wt%		20 wt% : 80 wt%		sym
F4	34 wt% : 66 wt%		66 wt% : 34 wt%		asy
F5	78 wt% : 22 wt%		22 wt% : 78 wt%		asy
F6	0 wt% : 100 wt%		0 wt% : 100 wt%		sym

Figure 3. Mechanical properties of symmetric and asymmetric polymer-lipid vesicles (A) (left) schematic illustration and (middle and right) optical microscope image of a vesicle being deformed in a micropipette by an incremental suction pressure, ΔP, until it ruptures. We detect the contours of the vesicle both inside and outside of the pipette, which allow us to determine, R_s and R_p, radii of the vesicle outside and inside of the pipette respectively, L, the length of the vesicle being sucked into the pipette, and A_o, the original spherical surface area of the vesicle. To calculate the areal strain, α, we use $\alpha = \frac{2\pi R_p L}{A_o}\left(1 - \frac{R_p}{R_s}\right)$. To calculate the tension, τ, in the membrane, we use $\tau = \frac{\Delta P}{2\left(\frac{1}{R_p} - \frac{1}{R_s}\right)}$. The experiment ends when the vesicle ruptures under the highest pressure. (B) table of formulations with composition estimation in each type of vesicles; F1 to F3 are sym vesicles containing increasing polymer contents; F4-F5 are two asy vesicles with different leaflet configuration and asymmetric degree; F6 is a pure polymersome group (C) Membrane tension versus areal strain curves. For symmetric vesicles, F1 to F3, increasing polymer content increases the stretching modulus of vesicles. For the asymmetric vesicle with lipid inner and polymer outer, F5, the vesicles are both stiff and stretchable as compared to sym groups F1 to F3, and stiffer than the asymmetric vesicles, with lipid outer and polymer inner, F4. (D) rupture of all types of vesicles reveals their liquid or solid like behaviors. F1, F2, and F4, which all contain amounts of lipids exceeding 40%, behave more like liquid vesicles without wrinkles at rupture. F3, F5, and F6, which either have more amounts of polymers, or likely a connected polymer leaflet, behave more like solid vesicles with wrinkles at rupture. (E), (F) Statistical summary of the stretching moduli and lysis strain across all vesicle types. The results show that asymmetric vesicles have medium stretching modulus and stiffness, which results (F) in its highest toughness among all vesicle types and its stiffness being half of the polymersomes.

Figure 4.

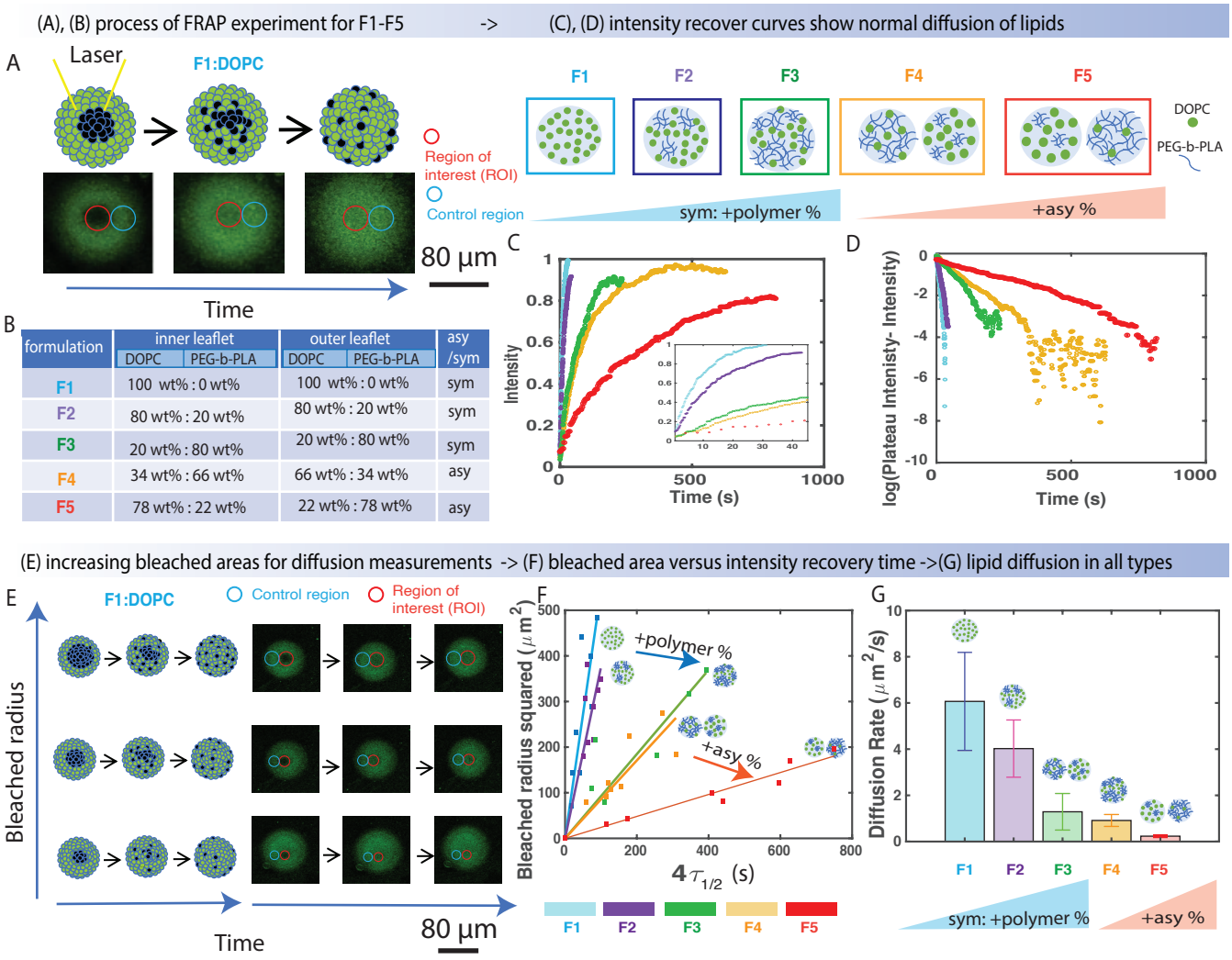

formulation	inner leaflet		outer leaflet		asy /sym
	DOPC	PEG-b-PLA	DOPC	PEG-b-PLA	
F1	100 wt% : 0 wt%		100 wt% : 0 wt%		sym
F2	80 wt% : 20 wt%		80 wt% : 20 wt%		sym
F3	20 wt% : 80 wt%		20 wt% : 80 wt%		sym
F4	34 wt% : 66 wt%		66 wt% : 34 wt%		asy
F5	78 wt% : 22 wt%		22 wt% : 78 wt%		asy

Figure 4. FRAP measurements of lipid diffusivity in symmetric and asymmetric polymer-lipid vesicles (A) (Top) schematic illustration and (bottom) optical images showing a laser photobleaching a circular area of a fluorescently labeled DOPC vesicle and the fluorescence recovers due to the diffusion of lipid molecules. (C) Fluorescence recovery in bleached area measured for a vesicle, with radius of approximately 10 um, of each vesicle type. The fluorescence intensity in the bleached area over time, I(t), is normalized to an intensity in the control area, which is of the same radius but unbleached, (D) log intensity of fluorescence recovery curves show normal diffusion of lipids. We plot the log plots of the recovery intensity and find they all behave linearly, indicating the lipids diffuse normally, allowing us to fit the recovery intensity to a simple equation, $I(t) = A(1 - \exp(-\frac{t}{\tau_D}))$ We obtain the lifetime of recovery, τ_D, and half time of recovery, $\tau_{1/2} = -(\ln 0.5)\,\tau$. The fluorescence fully recovers to 90% to 100% of the pre-bleached level as can be seen in the supplement. (E) process for bleaching vesicles with varied bleached radii (F) we plot the square of the radius of the bleached spot, r^2, versus the half time, $\tau_{1/2}$, which exhibit linear relationships. With increasing polymer content in symmetric vesicles, the slope decreases as shown by F1 to F3. With increasing asymmetry degree, the slope decreases even more as shown by F4 and F5. (G) The diffusion coefficients of the vesicles across various types are calculated from the slopes of the lines and represented in a bar plot. The highly asymmetric vesicles in V5 have much slower lipid diffusion coefficient than the symmetric vesicles in F1to F3.

Figure 5

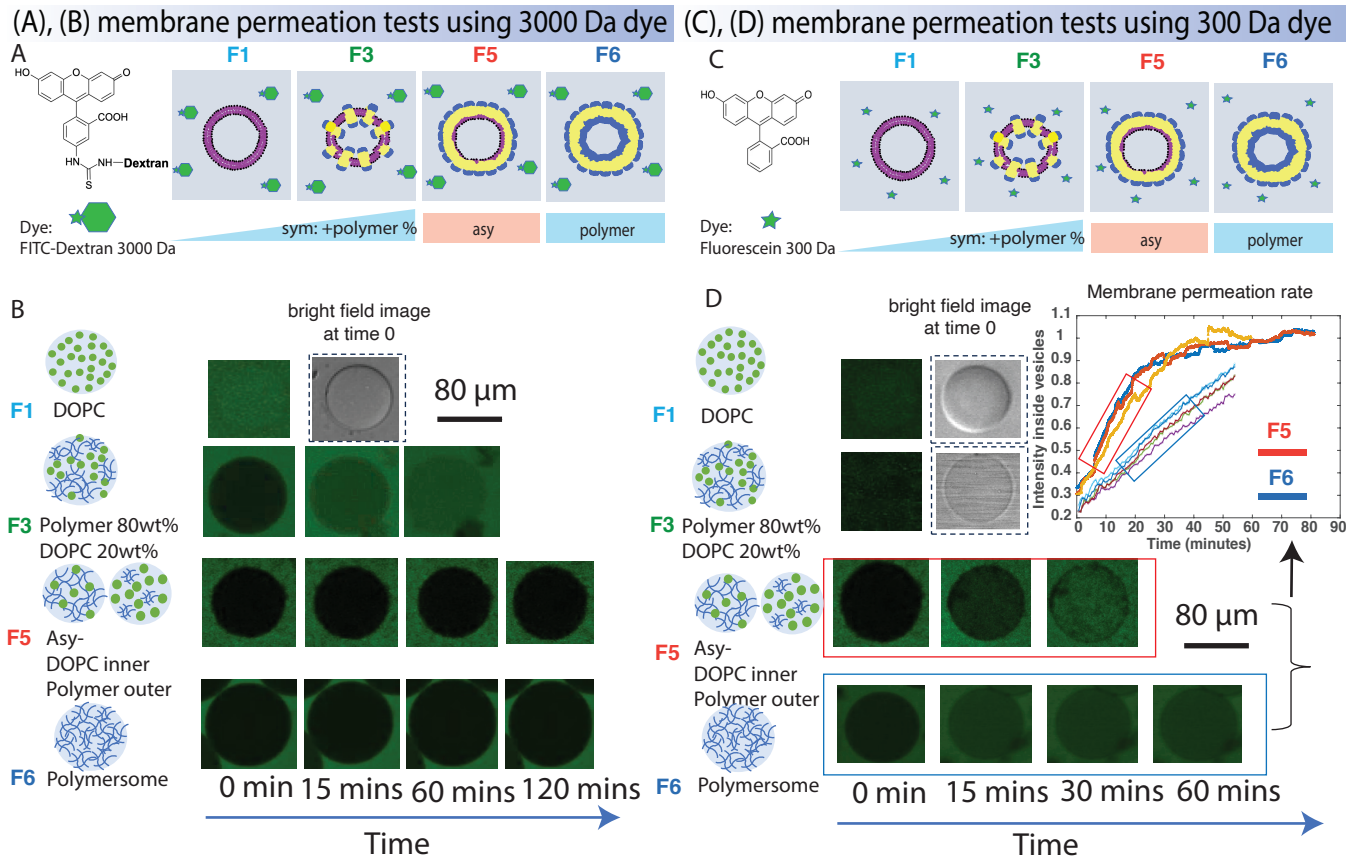

Figure 5 Diffusion of FITC-Dextran of 3000 Da and 300 Da into vesicles with various compositions. (A) schematic for testing membrane permeation using FITC-dextran 3000 Da. (B) Diffusion of FITC-dextran 3000 Da into different vesicle types with identical radii. First row: FITC-Dextran diffuses into DOPC vesicles and reaches saturation immediately after adding the dye. Second row: the dye gradually diffuses into symmetric vesicles containing 80 wt% polymers and 20 wt% lipids and reaches saturation after 60 minutes. Third row: no fluorescence is observed in the highly asymmetric vesicles with lipid inside and polymer outside for 120 minutes. Fourth row: no fluorescence is observed in the polymersomes for 120 minutes. These fluorescent images suggest the pore size of asymmetric vesicles is comparable to that of polymersomes and much smaller than that of the symmetric vesicles. (C)schematic for testing membrane permeation in different types of vesicles with identical radii, using FITC-dextran 300 Da. (D) First row: fluorescein diffuses into DOPC vesicles and reaches saturation immediately after adding the dye. Second row: similar as in DOPC vesicles, fluorescein diffuses into symmetric vesicles containing 80 wt% polymers and 20 wt% lipids and reaches saturation immediately after adding the dye. Third and row: fluorescein takes approximately 30 mins and 60 mins to diffuse into an asy vesicle, F5, with polymer outer and pure polymersome, F6, respectively. The plot (upper right) shows the intensity inside the asy vesicles, F5, increase approximately twice as fast as the pure polymersomes, F6, indicating the asymmetric vesicles likely possess a single polymer leaflet with approximately twice the diffusion constant and halved membrane thickness as compared to polymersomes.

Supplementary Information

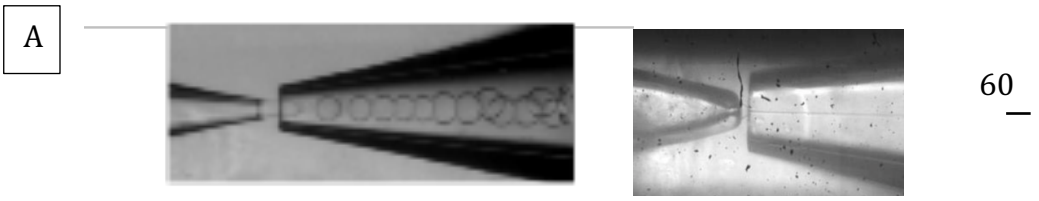

Fig S1. Microfluidic production of symmetric vesicles. (A) Production of vesicles with larger diameter of approximate 80 μm and (B) vesicles with smaller diameter of approximately 2 μm

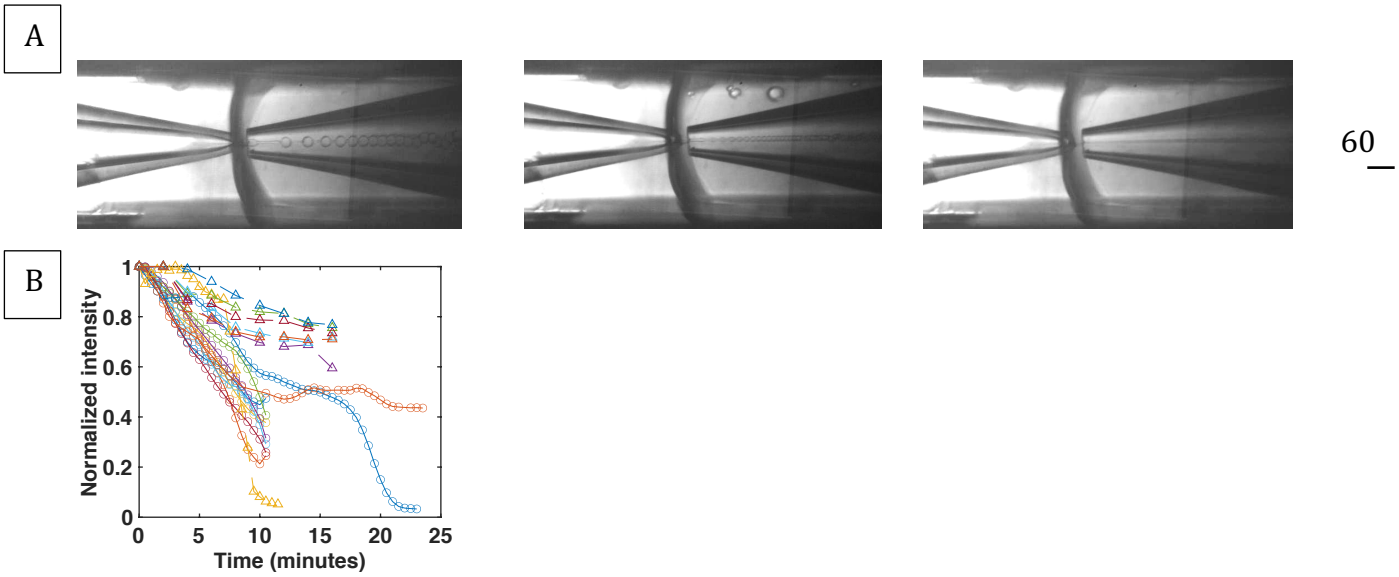

Fig S2. Microfluidic production of asymmetric vesicles. (A) Production of asymmetric vesicles with diameters of approximate 80 μm, 40 μm, and 2 μm from left to right. (B) Quenching experiments for vesicles with polymer outside and fluorescent NBD-PE lipid inside, represented by triangles, and vesicles with polymer inside and fluorescent NBD-PE lipid outside, represented by circles. The intensities of vesicles either get mostly quenched for polymer inside and lipid outside or plateaus for polymer outside and lipid inside, after approximately 10mins. We use the intensity at 10mins to calculate the degree of asymmetry for each types of vesicles.

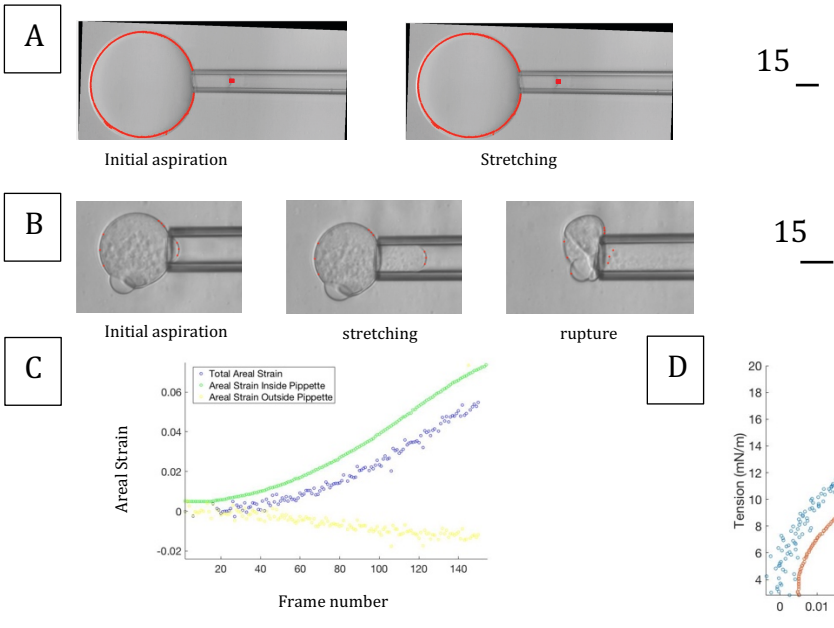

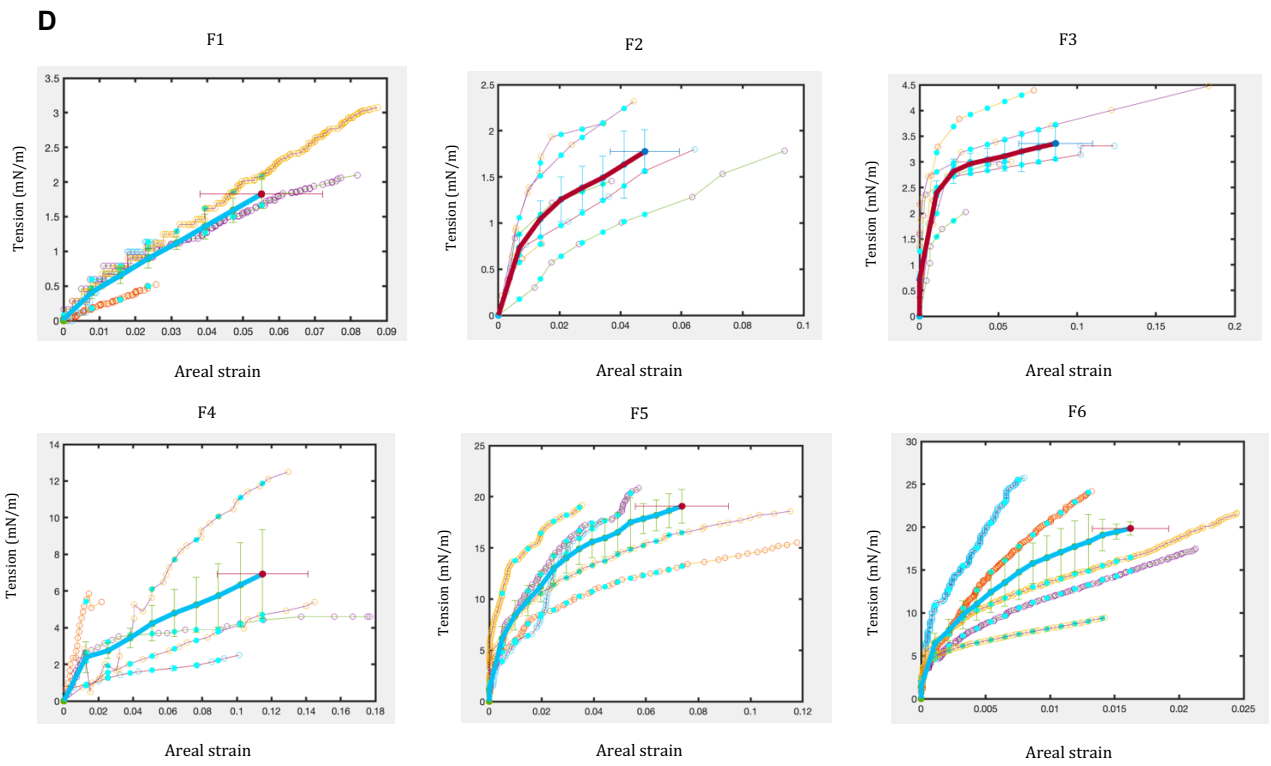

Fig S3. (A) We detect contours of vesicles outside of the pipette and length of the vesicle inside the pipette, we use that to project a 3D surface area and calculate the exact surface area. (B) We detect the radii of vesicles outside and inside of the pipette, as well as the length of vesicle inside the pipette. We use the equation, $\alpha = \frac{2\pi R_p L}{A_o}(1 - \frac{R_p}{R_s})$, to estimate the areal strain. (C) We show that the exact areal strain in (A) and estimated areal strain in (B) yield similar tension versus areal strain for a typical vesicle. Thus we can use the estimation equation in (B) for the measurement. (C) The highlighted colors indicate the average measurement from all vesicles in the group. Vesicles rupture at the maximum strain during the aspiration.

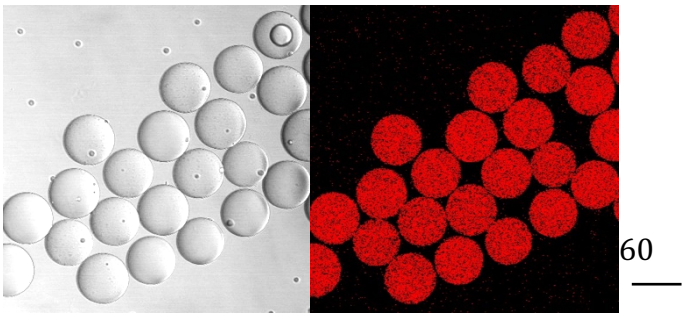

Fig S5: Encapsulation of doxorubicin inside vesicles. Asymmetric vesicles with polymer outside and lipid inside are shown.

Supplementary Information

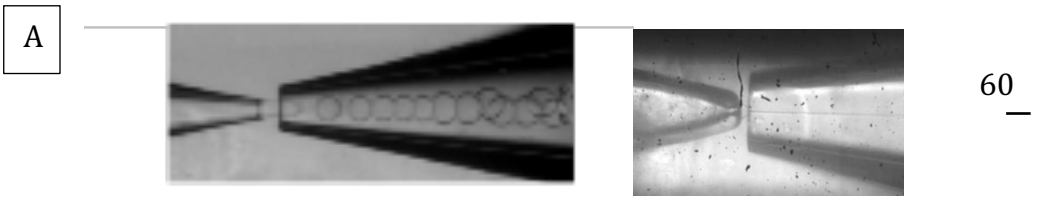

Fig S1. Microfluidic production of symmetric vesicles. (A) Production of vesicles with larger diameter of approximate 80 μm and (B) vesicles with smaller diameter of approximately 2 μm

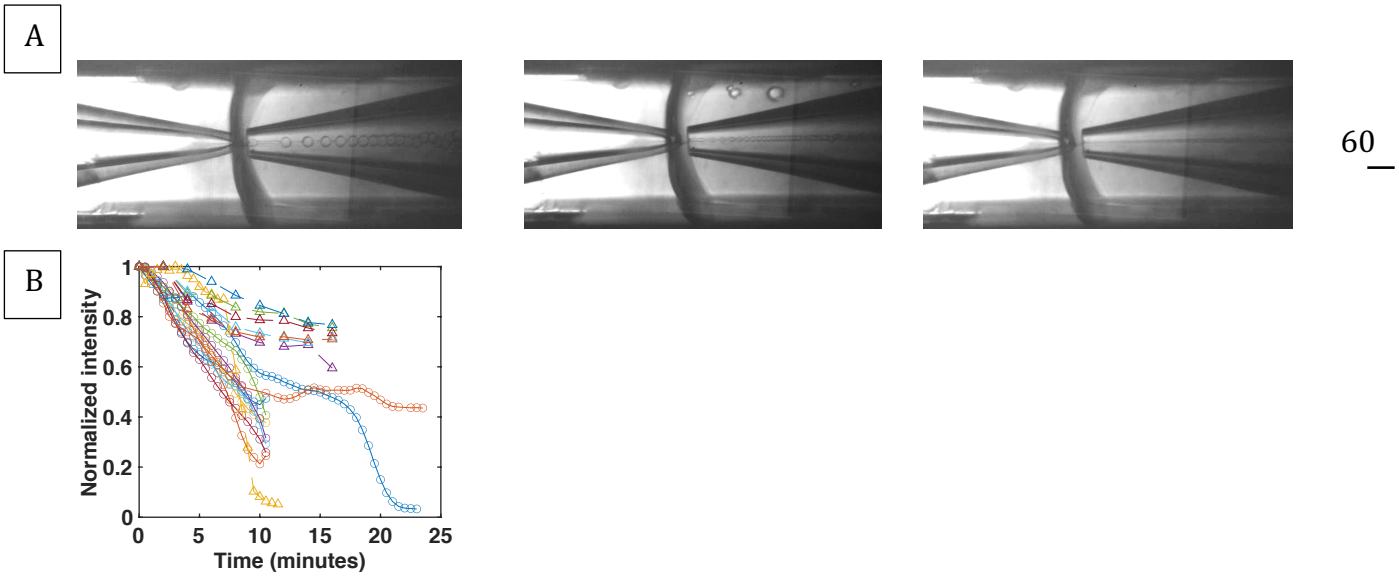

Fig S2. Microfluidic production of asymmetric vesicles. (A) Production of asymmetric vesicles with diameters of approximate 80 μm, 40 μm, and 2 μm from left to right. (B) Quenching experiments for vesicles with polymer outside and fluorescent NBD-PE lipid inside, represented by triangles, and vesicles with polymer inside and fluorescent NBD-PE lipid outside, represented by circles. The intensities of vesicles either get mostly quenched for polymer inside and lipid outside or plateaus for polymer outside and lipid inside, after approximately 10mins. We use the intensity at 10mins to calculate the degree of asymmetry for each types of vesicles.

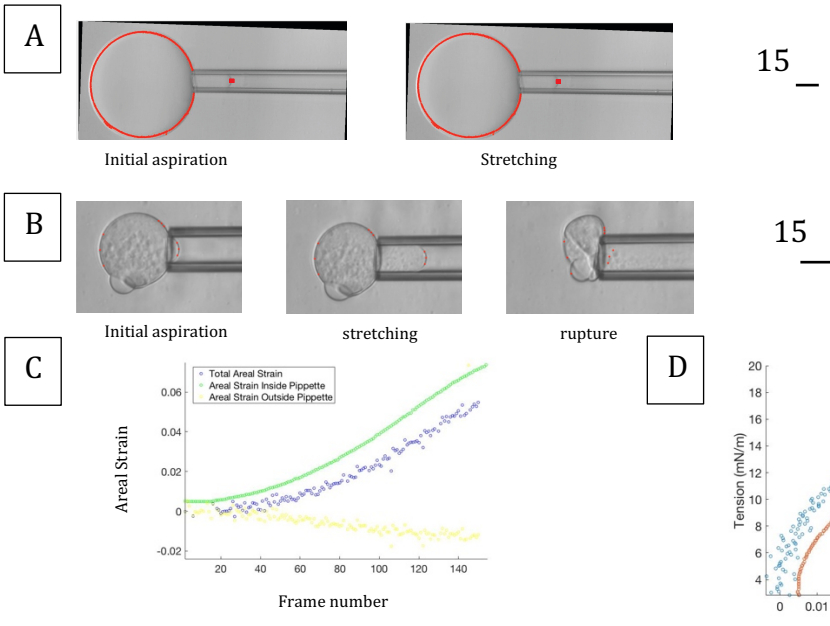

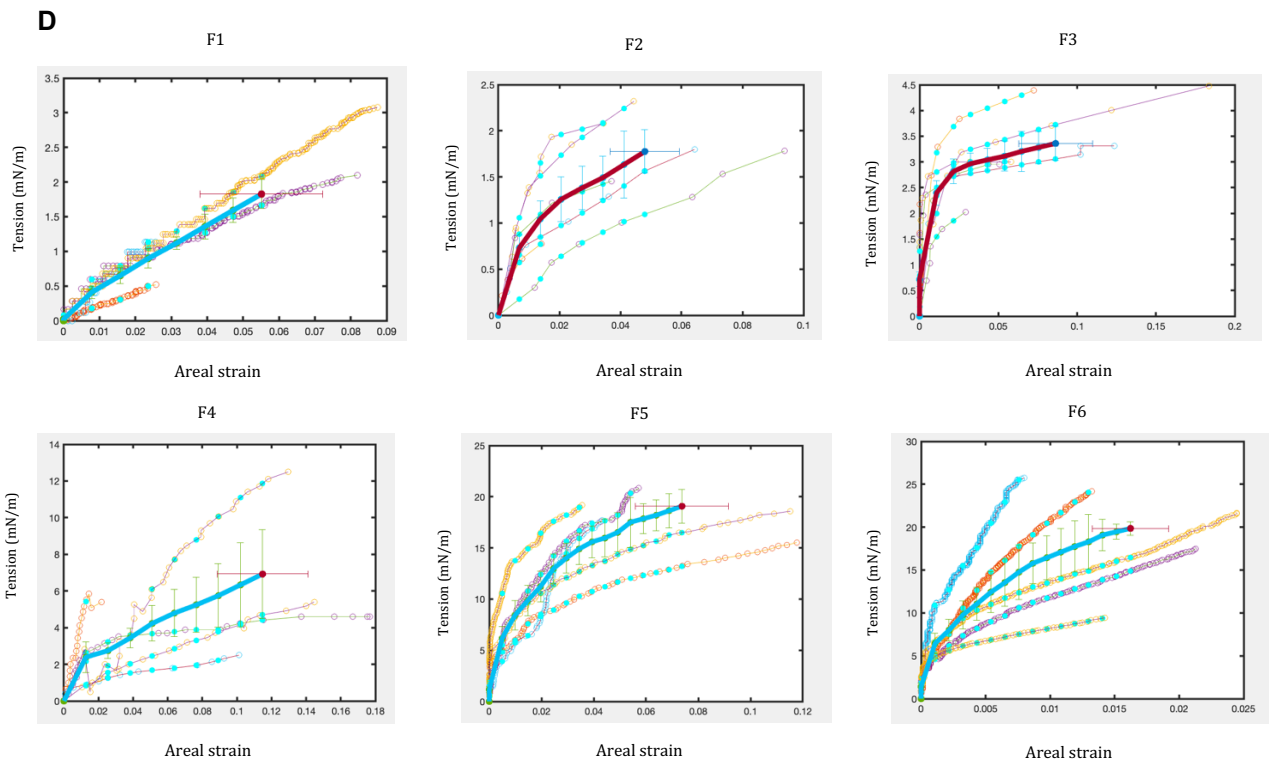

Fig S3. (A) We detect contours of vesicles outside of the pipette and length of the vesicle inside the pipette, we use that to project a 3D surface area and calculate the exact surface area. (B) We detect the radii of vesicles outside and inside of the pipette, as well as the length of vesicle inside the pipette. We use the equation, $\alpha = \frac{2\pi R_p L}{A_o}(1 - \frac{R_p}{R_s})$, to estimate the areal strain. (C) We show that the exact areal strain in (A) and estimated areal strain in (B) yield similar tension versus areal strain for a typical vesicle. Thus we can use the estimation equation in (B) for the measurement. (C) The highlighted colors indicate the average measurement from all vesicles in the group. Vesicles rupture at the maximum strain during the aspiration.

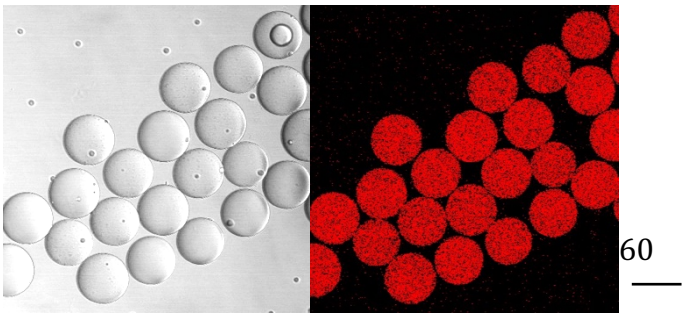

Fig S5: Encapsulation of doxorubicin inside vesicles. Asymmetric vesicles with polymer outside and lipid inside are shown.